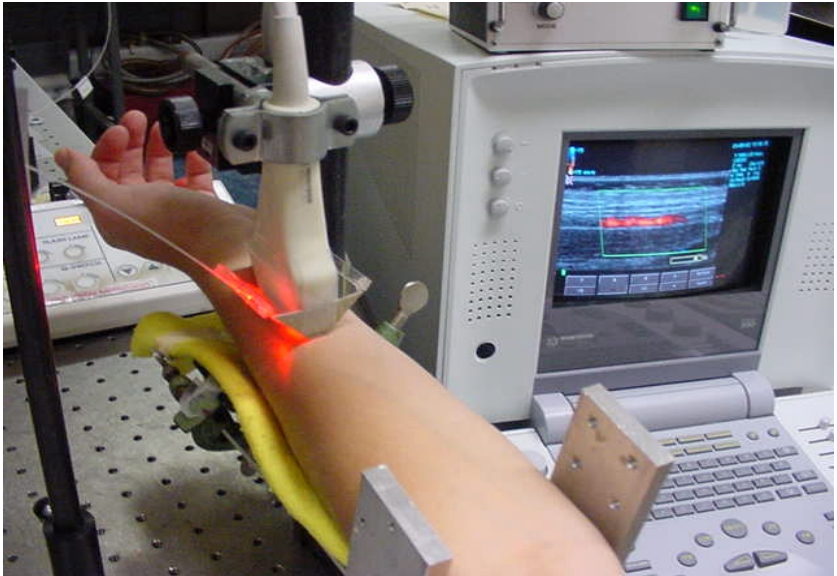# Real-Time Biomedical Optoacoustic Imaging

JOËL J. NIEDERHAUSER

2004

DISS. ETH NO. 15572

Real-Time Biomedical Optoacoustic Imaging

A dissertation submitted to the

SWISS FEDERAL INSTITUTE OF TECHNOLOGY ZURICH

for the degree of
Doctor of Technical Sciences

presented by

JOËL J. NIEDERHAUSER

Dipl. El.-Ing. ETH
born 4.7.1976
citizen of Böckten BL and Liestal BL

accepted on the recommendation of
Prof. P. Niederer, examiner
Prof. M. Frenz, co-examiner

2004

Contents

Abstract

In optoacoustic imaging, short laser pulses irradiate scattering biological tissue and adiabatically heat hidden absorbing structures, such as blood vessels, to generate pressure transients by means of the thermoelastic effect. These acoustic transients propagate to the tissue surface and are recorded with transducers to reconstruct high contrast images of the initial absorbed energy distribution exactly resembling the absorbing structures.

Two groups of new real-time optoacoustic imaging systems were developed: (1) Optical systems exploring Schlieren optical detection and acoustic lens system for 3D imaging. (2) Laser excitation combined with classical medical ultrasound system for comparison of the two complementary techniques. In medical applications real-time imaging avoids motion artifacts (heartbeat and breath), facilitates imaging procedure and allows instant diagnosis.

In the first optical system, the Schlieren transducer images the pressure transient in a fluid filled cuvette below the tissue with an ns-flash lamp and reconstructs images on a computer for visualization. The second optical system uses an acoustic lens to directly reconstruct a 3D image of the original pressure distribution into a water container. This copied pressure image is optically dark field imaged at two angles to provide a stereo image pair of the original absorbing structures. Both optical systems operate at real-time frame rates of 10-20 Hz and provide high resolutions up to 30-100 μm. Both systems allow illumination at the position of sensing through the transducer water tank (backward mode optoacoustic imaging). This is advantageous for all body parts not accessible from two opposite sides or containing bones. An additional part of basic research included piezoelectric ultrasound transducer design. Piezoelectric polyvinylidene-fluoride (PVDF) is widely established for high bandwidth single element transducers in optoacoustics. A new PVDF sensor for optoacoustic depth profiling featuring transparent conductive indium-tin-oxide electrodes (ITO electrodes) was developed, which allows backward mode operation and quantification of optical properties.

Medical ultrasound, a widely used diagnostic tool, is limited by low acoustic contrast, which particularly deteriorates or inhibits imaging of smaller structures in near skin regions. Two systems combining laser-excitation and commercial ultrasound are presented exploring high optical contrast and sub-millimeter acoustical spatial resolution for *in vivo* biomedical optoacoustic imaging. Variation of the laser wavelength allows spectroscopy and functional imaging of blood oxygenation level based on oxygen dependent hemoglobin absorption spectra. The sophisticated combined system features 64-channel parallel acquisition of an image using a single laser pulse. The online image reconstruction based on FFT takes 100 ms and therefore allows real-time operation. The *in vivo* optoacoustic images acquired from human finger, arm and legs show high contrast detailed blood vessel structures, which are hard to see on the corresponding ultrasound echography images. The two techniques extract complementary information, which strongly suggests a combination (overlay) of the two techniques in a single device.

In conclusion, real-time and 3D capability of optoacoustics has been demonstrated with the newly developed high contrast biomedical optoacoustic imaging systems.

Zusammenfassung

In der optoakustischen Bildgebung durchleuchten kurze Laserpulse streuendes, biologisches Gewebe und wärmen eingebettete, absorbierende Strukturen wie Blutgefässe, was zur Erzeugung von Drucktransienten führt (Thermoelastischer Effekt). Diese akustischen Transienten propagieren zur Gewebeoberfläche, wo sie mit Schallwandlern aufgenommen werden, um ein kontrastreiches Bild der absorbierenden Strukturen rekonstruieren zu können.

Zwei Gruppen von neuen, echtzeitfähigen optoakustischen Abbildungssysteme wurden entwickelt: (1) Optische Systeme mit Schlierenoptik und akustischer Linse für 3D Bildgebung. (2) Kombination von Laseranregung mit einem klassischen medizinischen Ultraschallgerät zum Vergleich der zwei komplementären Techniken. Bei medizinischen Anwendungen verhindern Echtzeitgeräte Bewegungsartefakte (Herzschlag und Atmung), vereinfachen den Untersuchungsablauf und liefern direkte Diagnosen.

Beim ersten optischen System bildet der Schlierendetektor die Drucktransienten in einer wassergefüllten Küvette unter dem Gewebe mit einer ns-Blitzlampe ab, rekonstruiert die Bilder und visualisiert sie auf einem Computer. Das zweite optische System benützt eine akustische Linse zur direkten Rekonstruktion eines 3D-Bildes der ursprünglichen Druckverteilung in einen Wasserbehälter. Die kopierte Druckverteilung wird mit einem optischen Dunkelfeldverfahren unter zwei Winkeln aufgenommen, um ein Stereo-Bildpaar der ursprünglichen absorbierenden Struktur zu erhalten. Beide optischen Systeme sind echtzeitfähig mit 10-20Hz Repetitionsraten und mit 30-100 μm örtlicher Auflösung. Bei beiden Systemen erfolgt die Lasereinstrahlung durch den Wasserbehälter an derselben Position wie die Detektion (Rückwärtsmodus). Das ist von Vorteil bei allen Körperteilen, die nicht von zwei gegenüberliegenden Seiten zugänglich sind oder Knochen enthalten. Ein weiterer Teil der Grundlagenforschung war die Ultraschall-Wandlerentwicklung. Das piezoelektrische Polyvinylidenfluorid (PVDF) wird häufig in breitbandigen Einzelelementwandlern

für Optoakustik verwendet. Es wurde ein neuer PVDF für optoakustische Tiefenprofilierung mit transparenten, leitenden Indium-Zinn-Oxid-Elektroden (ITO-Elektroden) entwickelt, der die Quantifizierung optischer Eigenschaften im Rückwärtsmodus ermöglicht.

Medizinischer Ultraschall, ein weitverbreitetes Diagnoseinstrument, ist durch den schwachen akustischen Kontrast limitiert, der speziell die Bildgebung kleiner Strukturen in Hautnähe verschlechtert oder gar verhindert. Es werden zwei Systeme vorgestellt, die Laseranregung und kommerzielles Ultraschallgerät kombinieren, um so den hohen optischen Kontrast und die akustische sub-Millimeter Auflösung für *in vivo* optoakustische Bildgebung ausnutzen. Variation der Laserwellenlänge ermöglicht Spektroskopie und funktionale Bildgebung des Blutoxygenierungsgrades mit Hilfe des sauerstoffabhängigen, optischen Absorptionsspektrums von Hämoglobin. Das ausgeklügelte, kombinierte System zeichnet 64 Kanäle parallel auf um ein Bild mit einem einzigen Laserpuls zu erhalten. Die online Bildrekonstruktion, basierend auf FFT, dauert 100 ms und erlaubt somit Echtzeitbetrieb. Die *in vivo* optoakustischen Bilder von menschlichen Fingern, Armen und Beinen zeigen kontrastreiche, detaillierte Blutgefässstrukturen, die auf den entsprechenden Ultraschallechobildern nur schwer zu erkennen sind. Die zwei Techniken zeigen komplementäre Informationen, was die Kombination der beiden Techniken auf einem einzigen Gerät nahelegt (übereinandergelegtes Bild).

Zusammenfassend wurde Echtzeit- und 3D-Fähigkeit von Optoakustik anhand der neu entwickelten, kontrastreichen, optoakustischen Bildgebungssystemen gezeigt.

Introduction

The medical need for high quality diagnostic images has motivated research on biomedical optoacoustic imaging [1–40], a new technique which combines the merits and most compelling features of optics and ultrasound. Among the established medical imaging devices, ultrasound is widely favored due to its convenient real-time display and easy handling. Fast image acquisition not only reduces motion artifacts caused by respiration or heartbeat but also allows instant accurate diagnosis. This thesis presents the development of optoacoustic imaging to real-time functionality.

Ultrasound imaging has been conquering the medical world for half a century. Moderate price range and fast imaging have brought the technique into most doctor's offices. The human bodies under investigation are not a static environment and dynamic movements present a challenge for every imaging technique. Looking at the temporal scales of some movements, the average human heartbeat rate is 60 bpm or 1 Hz and the breath frequency is about 10 breath cycles per minute. To avoid motion artifacts the image acquisition times should be at least 5 times faster than the fastest body movement. Ultrasound imaging excels with frame rates going above 100 Hz allowing temporally resolved investigation of the heart valve and of pulsed blood flow in the arteries. The real-time capability also allows the doctor to find crucial regions of interest and to instantly diagnose the investigated region. These merits have opened the way to many medical applications. Ultrasound offers a most valuable tool for every clinician at an affordable price. The contrast of ultrasound is, however, unfortunately low. This makes detailed interpretation of the images more difficult and less intuitive. Contrast agents may increase the poor contrast but they lead

to more complicated investigations. An additional technique exploiting intrinsic contrast would be highly desirable. The intrinsic optical contrast of blood and surrounding tissue, for example, is very high in the visible or near infrared range. Pure optical methods, however, are limited by scattering to either millimeter imaging depths (optical coherence tomography) or to poor resolution in the centimeter range for deeper imaging (optical tomography). Optoacoustics, on the other hand, as hybrid method provides the optical contrast without the handicap of poor resolution for a moderate price range. This thesis investigates the potential of optoacoustics as a high contrast medical imaging technique in extension of classical ultrasound and even explores the possibility of real-time 3D imaging.

A recent surge of research forecasts the impact of biomedical optoacoustic imaging in the fields of blood vessel investigation [1, 2, 8, 11, 29], tumor diagnostics [28] and mammography [12, 30]. Cancerous tissue has a higher need of blood supply, which changes the vascularization of the tissue and the local oxygenation level of the blood [41–45]. Hemoglobin, a main component of blood, has a specific absorption spectrum depending on its oxygenation level. Optoacoustics, probing optical properties, exploits high optical contrast for blood vessel imaging and even spatially resolved blood oxygenation estimation.

In biomedical optoacoustics, tissue is illuminated with short laser pulses. The light is scattered inside the tissue and heats (by degrees or fraction of degrees) absorbing structures such as blood vessels. By means of the thermoelastic effect, the heating generates pressure transients exactly representing the absorbing structures. These ultrasound transients propagate to the tissue surface and are measured with an acoustic transducer.

There are several expressions that essentially describe the same technique and can cause confusion. The terms photoacoustics, optoacoustics, laser-induced ultrasound and thermoacoustics are almost interchangeable apart from nuances. Photoacoustics is the original name of the technique introduced by Bell [46] and describes the conversion from light to sound. Optoacoustics is a synonym to photoacoustics and originates from the two involved fields optics and acoustics. Laser-induced or laser generated ultrasound additionally specifies the use of lasers as a light source. Thermoacoustics stresses the sound generation by thermoelastic effect in contrast to other rarely used or weak conversions and is not restricted to

optical sources (e.g. microwave excitation).

The history of photoacoustics (optoacoustics) dates back to the 19th century [46], when A. G. Bell presented his invention, the photophone, an early wireless communication device. He used modulated sunlight to transmit spoken messages. The modulated beam was focused on a black absorber, sponge-like material, resulting in periodical heating and expansion of the surrounding air. The receiver could therefore hear the original message. The usability of the device was limited by the light source, the sun, which was one of the best mobile strong light sources available back then. Even though a first prototype of the system seemed to work, it could not compete with the spreading wired telegraph and telephone. The photoacoustic effect disappeared from research for want of a better light source.

With the invention of the laser in the sixties, new high power light sources became available. The photoacoustic research was revived with a first focus on chemical spectroscopy of gases. With periodic optoacoustic excitation at the resonant frequency of the gas container and lock-in detection these devices can trace very small concentrations down to PPB levels [47–53].

Non destructive testing (NDT) also discovered laser-induced ultrasound or photoacoustics as a broadband ultrasonic reference source [54–72]. With the advantages of non-contact operation and optical source shaping, laser-induced ultrasound has a wide range of applications. It serves as a standard reference and can be used for high frequency echography.

In medicine, lasers were first used in ophthalmology, a field historically associated with optics. Later on lasers were use as surgery tools for cutting and in cosmetic surgery for hair and tattoo removal. When used for cutting, the ablative laser pulses emit a well audible noise. This was one of the phenomena that inspired biomedical research to focus on optoacoustics. One-dimensional optoacoustic signals contain quantitative information on optical tissue properties. By scanning of the transducer, simple two-dimensional images can be reconstructed.

A key element of every optoacoustic system is the ultrasound transducer. Classically ultrasound transducers are made from piezoelectric materials, which allow a direct conversion of pressure into voltage. Piezo-

electric materials, such as Lead Zirconate Titanate (PZT), have high conversion efficiency. The ceramic transducers have a high sensitivity but a narrow band frequency response. In 1969 Polyvinylidene Fluoride (PVDF) was discovered to show piezoelectric properties [73, 74]. Its acoustic impedance is closer to water and it is therefore ideally suited for construction of wideband transducers. Medical ultrasound applications have motivated development of linear and even two-dimensional arrays. Manufacturing difficulties, however, limit the minimal element size and element number of such probes. These limitations have motivated research into new optical methods for detection of laser-generated ultrasound [4, 19, 21, 26, 31].

The optoacoustic imaging systems proposed so far [1, 3–6, 10–16, 21–31, 36–38] require scanning and time-consuming off-line image reconstruction. With long acquisition times, motion artifacts introduce loss of spatial resolution and make the systems more difficult to use. The novel systems proposed in this thesis overcome these limitations by providing images at real-time repetition rates.

Part 1 focuses on fundamental research and shows two optoacoustic imaging systems based on optical detection. The first uses direct Schlieren optics and the second uses an acoustic lens system. The acoustic lens system even goes one dimension further and provides 3D optoacoustic imaging in real-time. Also a transparent PVDF transducer is proposed which allows direct through illumination with the sound-generating laser.

Part 2 focuses on sophisticated *in vivo* optoacoustic imaging systems and their comparison with ultrasound echography. Three studies using conventional medical ultrasound devices for detection are presented. The first *in vivo* study describes safety limitations of optoacuostics, the second shows functional optoacoustic imaging using two irradiation wavelengths and the third proposes a real-time high contrast optoacoustic imaging system. The studies show the high optoacoustic contrast and suggest optoacoustics as a complementary technique, which could be ideally combined with existing ultrasound systems.

Optoacoustic theory with examples

The physical principle behind optoacoustics can be derived from basic equations. The major difficulty for optoacoustic research is that optoacoustics merges two historically separated fields of research, optics and ultrasound, which complicates notation and finding experts that are competent in both fields.

For generality a three-dimensional model using lateral dimensions x and y and depth z needs to be considered for optoacoustics.

In optoacoustics, biological tissue is homogenously irradiated with a short laser pulse of energy E [J] on an area A [m^2] leading to a radiant exposure [J/m^2]

$$H_0(x, y, z = 0) = \frac{E}{A} \tag{1}$$

on the surface.

The light is scattered and absorbed by the tissue. The optical tissue properties can be modelled with the local scattering coefficient $\mu_s(x, z, y)$, the anisotropy $g(x, y, z)$ and the absorption coefficient $\mu_a(x, y, z)$. A Monte Carlo simulation can compute the exact local exposures $H(x, y, z)$. If, for simplicity, homogeneous optical properties and predominant scattering are assumed, the problem can be solved analytically using the diffusion approximation, with the diffusion coefficient proportional to the reduced scattering coefficient $\mu_s' = \mu_s(1 - g)$. In the diffusion approximation for broad illumination the depth illumination eventually decreases exponentially with an effective attenuation coefficient

$$\mu_{eff} = \sqrt{3\mu_a(\mu_a + \mu_s')}. \tag{2}$$

The radiant exposure for large depths then becomes

$$H(x, y, z) \propto H_0 e^{-\mu_{eff} \cdot z}. \tag{3}$$

The optoacoustic stress generation depends on the locally absorbed or deposited volumetric energy density [J/m^3]

$$W(x, y, z) = \mu_a(x, y, z)H(x, y, z). \tag{4}$$

With density ρ [kg/m^3] and specific heat C_p [J/(kg °C)] this leads to a temperature increase [°C]

$$\Delta T(x, y, z) = \frac{W(x, y, z)}{\rho \cdot C_p}, \tag{5}$$

which, using expansivity β [strain per °C], would cause a volume expansion

$$\frac{\Delta V}{V} = \beta \Delta T. \tag{6}$$

However, if the original laser pulse is short enough, instead of the initial volume expansion, a local stress transient p_0 [Pa] is induced using the bulk modulus M [Pa per strain]

$$p_0(x, y, z) = M \frac{\Delta V}{V}. \tag{7}$$

Combining equations (4-7) we get

$$p_0(x, y, z) = \frac{M\beta}{\rho C_p} \mu_a(x, y, z) H(x, y, z). \tag{8}$$

The constants for water at room temperature of 20 °C are $M = 2.18 \cdot 10^9$ Pa, $\beta = 206 \cdot 10^{-6}$ °C^{-1}, $\rho = 1000$ kg/m^3 and $C_p = 4180$ J/kg°C. For water at body temperature of 37 °C the bulk modulus and expansivity change to $M = 2.26 \cdot 10^9$ Pa and $\beta = 362 \cdot 10^{-6}$ °C^{-1} [75]. The four material constants can be combined in the unitless Grüneisen coefficient $\Gamma = 0.11$ at 20 °C and $\Gamma = 0.19$ at 37 °C, which leads to

$$p_0(x, y, z) = \Gamma \cdot \mu_a(x, y, z) H(x, y, z) = \Gamma \cdot W(x, y, z). \tag{9}$$

This direct efficient conversion to pressure is possible if the acoustic transient does not leave the heated region during the heating process. This condition is called stress confinement and is satisfied if the pulse duration t_p is smaller than the propagation time of the acoustic transient through the region d with acoustic velocity c

$$t_p < d/c. \tag{10}$$

The size of the region d is either determined by the extend of the smallest absorbing structure or by the optical penetration depth $\delta = 1/\mu_{eff}$.

Now the conversion to acoustic transients is finished and the acoustic propagation can be modelled with the differential wave equation

$$\frac{\partial^2 p}{\partial t^2} = c^2 \nabla^2 p \tag{11}$$

and the initial condition

$$p(x, y, z, t = 0) = p_0(x, y, z). \tag{12}$$

The forward propagation can be calculated using either time domain or frequency domain (Fourier acoustics) methods.

In real tissue scattering is weak and acoustic velocity can be assumed constant as a first approximation. The undisturbed propagation by this approximation is only influenced by the frequency dependent attenuation in real tissue, which preferably attenuates high frequency content and therefore leads to reduction of spatial resolution.

The propagated transients are recorded outside the tissue to reconstruct an image of the original absorption distribution or to quantify optical properties of the tissue by fitting exponential slopes to one-dimensional signals.

The deposited heat reduces by thermal diffusion processes and by active transport of the blood flow. According to laser safety standard ANSI Z136.1 for the visual spectrum (400-700 nm), the maximal continuous irradiation on skin is 0.2 W/cm^2, while the maximum permissible exposure of a single pulse is 0.02 J/cm^2. These two values empirically indicate that at repetition rate of 10 Hz the heat deposition processes and heat diffusion/transport processes of the body are balanced.

To get a feeling for the optoacoustic transient generation two examples are given:

1. A laser pulse with energy $E = 40$ mJ, pulse length $t_p = 5$ ns, beam area $A = 2$ cm^2 and wavelength $\lambda = 570$ nm irradiates human blood with an absorption coefficient $\mu_a = 250$ cm^{-1}.

The radiant exposure (1) is

$$H_0 = \frac{E}{A} = \frac{40 \text{ mJ}}{2 \text{ cm}^2} = 20 \text{ mJ/cm}^2,$$

which is exactly the ANSI limit for for pulsed laser irradiation. According to (4) the absorbed volumetric energy density is

$$W = \mu_a H_0 = 250 \text{ cm}^{-1} \cdot 20 \text{ mJ/cm}^2 = 5000 \text{ mJ/cm}^3 = 5 \cdot 10^6 \text{ J/m}^3.$$

With physical constants for water this leads to a small temperature increase (5) of

$$\Delta T = \frac{W}{\rho \cdot C_p} = \frac{5 \cdot 10^6 \text{ J/m}^3}{10^3 \text{ kg/m}^3 \cdot 4.18 \cdot 10^3 \text{ J/kg°C}} = 1.2 \,°\text{C}$$

With $\Gamma = 0.2$ the generated initial pressure (7) is

$$p_0 = \Gamma \cdot W = 0.2 \cdot 5 \cdot 10^6 \text{ J/m}^3 = 1 \cdot 10^6 \text{ J/m}^3 = 1 \text{ MPa} = 10 \text{ Bar}$$

To get this high pressure, stress confinement (10) with a region $d = 1/\mu_a = 40 \,\mu\text{m}$ and sound velocity $c = 1.5 \,\mu\text{m/ns}$ needs to be satisfied

$$t_p = 5 \text{ ns} < d/c = \frac{40 \,\mu\text{m}}{1.5 \,\mu\text{m/ns}} = 27 \text{ ns} \checkmark$$

The theoretical achievable spatial resolution with the laser pulse length $t_p = 5$ ns is

$$t_p \cdot c = 5 \text{ ns} \cdot 1.5 \,\mu\text{m/ns} = 7.5 \,\mu\text{m}$$

which corresponds to a flat ultrasound frequency response up to a cut-off frequency of

$$f_c = \frac{1}{2t_p} = 100 \text{ MHz}.$$

The optoacoustic contrast between blood $\mu_a = 250 \text{ cm}^{-1}$ and bloodless surrounding tissue $\mu_{at} = 0.1 \text{ cm}^{-1}$ is

$$\frac{\mu_a}{\mu_{at}} = 2500 : 1 = 67 \text{ dB}.$$

At this wavelength range, very high contrast and spatial resolutions are achieved. The absorption of the light in the dermal vascularization however leads to lower exposures of deeper structures.

2. A laser pulse with energy $E = 100$ mJ, pulse length $t_p = 60$ ns, beam area $A = 5$ cm^2 and wavelength $\lambda = 760$ nm is irradiated on human tissue with homogeneous optical properties ($\mu'_s = 10$ cm$^{-1}, \mu_a = 0.1$ cm^{-1}) and an embedded vein in $z = 5$ mm depths ($\mu_a = 8.4$ cm^{-1}).

The radiant exposure (1) is

$$H_0 = \frac{E}{A} = \frac{100 \text{ mJ}}{5 \text{ cm}^2} = 20 \text{ mJ/cm}^2,$$

which is exactly the ANSI limit for for pulsed laser irradiation.

The effective attenuation coefficient of the bloodless tissue (2) is

$$\begin{aligned} \mu_{eff} &= \sqrt{3\mu_a(\mu_a + \mu'_s)} \\ &= \sqrt{3 \cdot 0.1 \text{ cm}^{-1} \cdot (0.1 \text{ cm}^{-1} + 10 \text{ cm}^{-1})} = 1.7 \text{ cm}^{-1}. \end{aligned}$$

With (3) the radiant exposure of the blood is in the order of

$$H \approx e^{-\mu_{eff} \cdot z} H_0 = e^{-1.7 \cdot 0.5} H_0 = 0.4 H_0 = 8 \text{ mJ/cm}^2.$$

The corresponding absorbed volumetric energy density (4) in the vein is

$$W = \mu_a H = 8.4 \text{ cm}^{-1} \cdot 8 \text{ mJ/cm}^2 = 67 \text{ mJ/cm}^3 = 67 \cdot 10^3 \text{ J/m}^3.$$

With physical constants for water this leads to a very small temperature increase (5) of

$$\Delta T = \frac{W}{\rho \cdot C_p} = \frac{67 \cdot 10^3 \text{ J/m}^3}{10^3 \text{ kg/m}^3 \cdot 4.18 \cdot 10^3 \text{ J/kg°C}} = 0.014 \text{ °C}$$

With $\Gamma = 0.2$ the generated initial pressure (7) is

$$p_0 = \Gamma \cdot W = 0.2 \cdot 67 \cdot 10^3 \text{ J/m}^3 = 13 \cdot 10^3 \text{ J/m}^3 = 13 \text{ kPa} = 0.13 \text{ Bar}$$

To get this pressure, stress confinement (10) with a region $d = 1/\mu_a = 1.2$ mm and sound velocity $c = 1.5$ mm/μs needs to be satisfied

$$t_p = 60 \text{ ns} < d/c = \frac{1.2 \text{ mm}}{1.5 \text{ mm}/\mu s} = 790 \text{ ns } \checkmark$$

The theoretical achievable spatial resolution with the laser pulse length $t_p = 60$ ns is

$$t_p \cdot c = 60 \text{ ns} \cdot 1.5 \text{ } \mu\text{m/ns} = 90 \text{ } \mu\text{m}$$

which corresponds to flat ultrasound frequency response up to a cut-off frequency of

$$f_c = \frac{1}{2t_p} = 8.3 \text{ MHz}.$$

The optoacoustic contrast between blood $\mu_a = 8.4$ cm^{-1} and bloodless surrounding tissue $\mu_{at} = 0.1$ cm^{-1} is

$$\frac{\mu_a}{\mu_{at}} = 84 : 1 = 38 \text{ dB}.$$

At this wavelength range, larger imaging depths are achieved while keeping good contrast and spatial resolution.

Optoacoustics compared to other medical imaging techniques

Biomedical optoacoustics has the advantages of providing high contrast images using non-ionizing laser irradiation and costing little.

X-ray imaging and computer tomography (CT) are major medical imaging methods. Their X-ray radiation, however, is ionizing and increases cancer risk when applied in large doses to biological tissue. This

drawback prohibits preventive frequent mammography screening of the whole female population. X-rays can penetrate the whole body and shows the bones with high contrast. To see blood vessels, however, contrast agents are used. Optoacoustics on the other hand cannot penetrate the whole body, but its visible light is non-ionizing and shows detailed blood vessels without contrast agents.

Magnetic Resonance Imaging (MRI) is a powerful imaging technique that has found wide acceptance because of the impressive image quality it provides. To get good images, however, large magnetic fields in the Tesla range are required, which require expensive technology and special facilities. Usually only the large hospitals can afford MRI and the high cost limits its use to special applications. Optoacoustic imaging can not compete with MRI image quality in these special applications, but it can offer an insight into shallower regions for a lower price.

Ultrasound is widely used in clinics because of its real-time capability and its low price. The low acoustic contrast, however, complicates interpretation of the images and requires extensive training of the investigators. Optoacoustics does not penetrate to the decimeter depths of ultrasound, but it offers much higher contrast for the first centimeters. The financial investment for optoacoustics is slightly higher but comparable to ultrasound as the receiver hardware can be identical.

Optical Tomography (OT) offers high optical contrast but has not made its way to clinics yet because of the poor spatial resolution. The spatial resolution can be increased by Time of Flight (TOF) techniques, which, however, require very expensive laser system. Optoacoustics, which is also based on optical contrast, offers the same imaging depths of a few centimeters as OT and TOF but provides good spatial resolution for a low price.

Optical Coherence Tomography (OCT) uses low coherence light sources to get excellently resolved images from the first millimeter depths. The high optical contrast and good spatial resolution has started to bring OCT to clinical application. Optoacoustics, targeting centimeter depths, can therefore optimally fill the gap between Ultrasound and OCT by providing high contrast images for medium depths at moderate cost.

Discussion and outlook of the thesis

The initial goal of my PhD project was the development of optoacoustic imaging to a state allowing real medical applications.

This goal has been reached with the new systems. High contrast optoacoustic imaging was combined with classical ultrasound to a new imaging system at convenient real-time frame rates providing a new insight into the human body *in vivo*. In addition, the feasibility of real-time 3D imaging has been demonstrated. The technical difficulties have been solved. The transfer to and the acceptance by the medical community, however, proved more difficult and time consuming than initially assumed.

One next step for the combined optoacoustic ultrasound system would be a medical research study on tumors, smoker's leg or anaesthesia surveillance. The study would be conducted in collaboration of a medical researcher and a physicist/engineer. This study could demonstrate the value of the new method as a diagnostic tool for the mentioned fields.

A major challenge of the optical detection systems is their lower sensitivity compared to piezoelectric systems. This limitation is caused by the common trade-off between sensitivity and spatial resolution of a detector. Increase of sensitivity by increasing or amplifying of the probing light would be necessary for *in vivo* applications. Unlike other optical methods which are restricted by saturation of the photodiodes, the optical methods in this thesis are based on dark field imaging and therefore allow an increase of probing beam intensity that has not been fully exploited yet. So another next step would be the exploration of this potential and the improvement of the optical detection towards a clinically applicable device.

Another way would be that a major ultrasound company would discover and incorporate the optoacoustic technology, whose feasibility has been shown in this thesis, into one of their commercial ultrasound systems. The slight cost increase of such a device would be outshone by the major gain of contrast in the images. Providing medical doctors with this augmented information could initiate a wide surge of demand for this new valuable technology.

Part I

Basic research to real-time 3D optoacoustic imaging

Chapter 1

Real-time optoacoustic imaging using a Schlieren transducer

Real-time optoacoustic imaging using a Schlieren transducer

Abstract

Optoacoustics, which combines the merits and most compelling features of light and sound, is a novel technique for diagnosing optical tissue properties and for performing non-invasive medical imaging. We present a detection method based on Schlieren optical imaging used to record optoacoustic waves generated with 6 ns long laser pulses. These waves result from irradiation of optically absorbing targets hidden deep inside highly scattering media. Since generated from one single shot, Schlieren images contain all the information necessary for the reconstruction of the absorbing structures. The detection method allows on-line imaging with a spatial resolution of about 30 μm with high contrast. The proposed real-time imaging system not only enhances the level of visible detail but it is ideally suited for monitoring dynamic tissue changes.

Recent interest in novel non-invasive medical diagnostic systems has motivated research into optoacoustic systems.[1] Generating ultrasonic waves with short laser pulses inside biological tissue, optoacoustics combines the merits of both, ultrasound and optics.[1-3] Producing high contrast at medium depths, optoacoustic methods have the potential to close the gap between high resolution optical coherence tomography[4] and conventional ultrasound in medical imaging. To become accepted as diagnostic medical imaging technique, optoacoustic methods should provide images in real time. A prerequisite for real time optoacoustic imaging is a fast detection of laser-generated pressure waves combined with a fast image reconstruction algorithm. Piezoelectric transducers are widely used for the detection of ultrasound.[3,5,6] Despite their high sensitivity, piezoelectric detection systems are limited in either resolution (manufacturing limitations for fine-pitched arrays) or in speed (mechanical scanning of a focused transducer). Various two-dimensional (2D) optical detection arrays have been described to overcome these resolution limitations.[7-9] The problem for real-time operation of the optical detection methods, however, is the desired high camera frame rate of about 10 MHz. The goal of this study was to develop a novel pressure detection which combines the high resolution of an optical

Schlieren detection with the real-time quality of a one-dimensional (1D) array transducer. Originating back to the 17th century, Schlieren imaging visualizes pressure gradients with high resolution and high sensitivity.[10,11] Our optoacoustic system uses one single Schlieren image to reconstruct pressure sources inside a sample, which allows real-time imaging of absorbing structures inside a scattering media such as tissue.

Figure 1 shows the schematics of the optoacoustic imaging setup. The pressure waves were generated with 5 ns optical parametric oscillator (OPO) laser pulses at a repetition rate of 10 Hz, delivered through a 600 μm fiber. The Schlieren optical system detected the pressure waves in a fluid filled cuvette at a predetermined moment after the exciting laser pulse ($\Delta t = 7$ μs). The illumination of the cuvette was done with a parallel beam of a 35 ns flash lamp passed through a 50 μm slit and collimated by a spherical mirror with a focal length of 1 m. The sensitivity of the system could be increased by propagating the illuminating beam twice through the cuvette (the back of the cuvette is a reflecting mirror). A razor blade was put into the focus generated by the spherical mirror to block the deflected beam. The Schlieren images were captured by a charge coupled device (CCD) camera and stored on a personal computer (PC) for further processing. It has to be mentioned that the reconstruction is accomplished using one single CCD image. A 3 μm mylar foil covering the cuvette, separated the filling fluid from the ultrasound gel used to guarantee a good acoustic contact to the sample. Two different liquids were used in the cuvette: (1) Water, which results in a low sensitivity but allows an accurate fast Fourier-transform (FFT) 2D-deconvolution algorithm for reconstruction of the absorbing objects. (2) Perfluorcarbonliquid (C_6F_{14}), which gives a three times higher sensitivity due to the three times lower sound velocity, but requires a time of flight algorithm for reconstruction of the absorbing objects because of acoustic refraction on the surface of the detection cuvette. In both cases, a linux PC (1 GHz Pentium III) reconstructed and visualized the source distribution in less than 50 ms based on the measured bipolar Schlieren image signal. The reconstruction algorithms assume homogeneous acoustic properties of the surrounding medium and ignore acoustic scattering.To demonstrate the sensitivity and the speed of the Schlieren-optical detection system, we placed two 0.5 mm graphite pencil leads parallel with a distance of 1 mm into the ultrasound gel above the cuvette. Figure 2 shows the original Schlieren image as captured with the CCD camera, which was used to reconstruct the absorbing
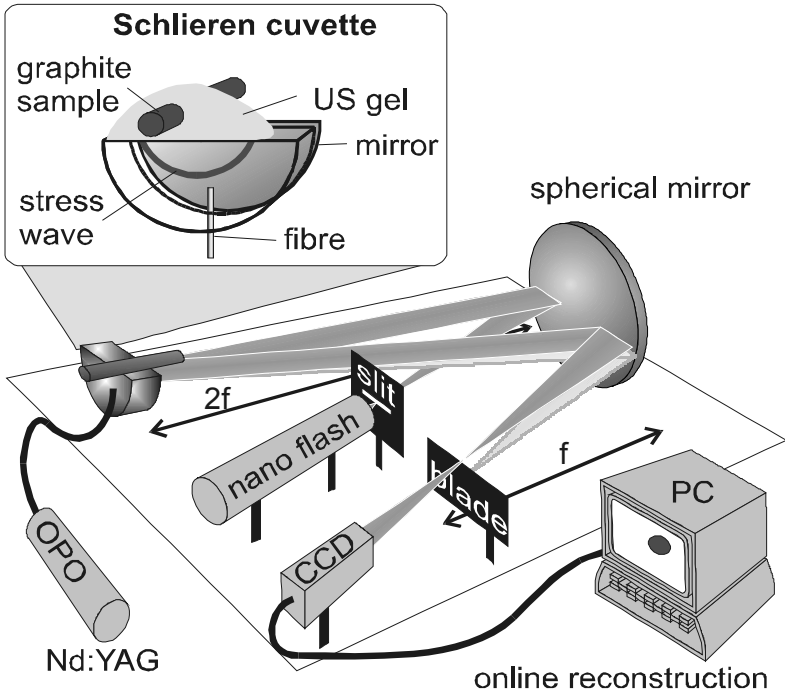
FIG. 1. Setup of the real-time optoacoustic imaging experiment. Laser generated stress waves in the cuvette were measured using a Schlieren method. The inlet shows the Schlieren-image transducer cuvette with the sample on top. US Gel= Ultrasound gel matching the acoustic impedance of biological tissue.

shape of the test sample (Figure 3). With a complete reconstructed image every 50 ms, any movement and rotation of the graphite sample could be visualized in real-time on the screen.

To compare the sensitivity of the novel Schlieren optical pressure detection system to that of a ring piezo-electrical transducer (polyvinylidene fluoride; PVDF),[12] we illuminated the same test sample with exactly equivalent laser parameters. Identical signal to noise ratios were obtained when using laser pulse energies of 100 µJ for the Schlieren setup and 3 µJ for the piezo setup. The sensitivity of a piezo transducer is proportional to its active area, which was more than 20
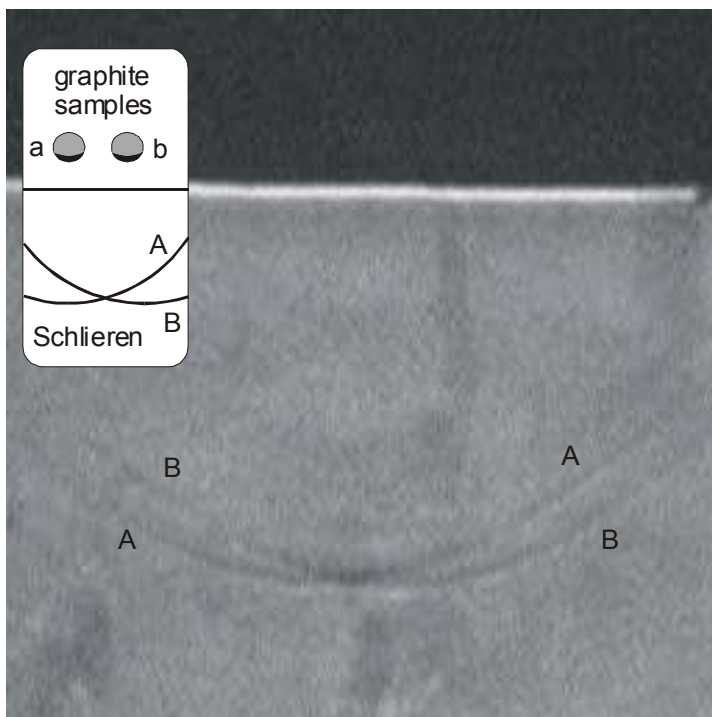
FIG. 2. Schlieren image showing the refractive index gradients inside the cuvette caused by the laser irradiated graphite samples (a and b). The absorbing volume of the graphite samples is marked dark in the inlet. The two bipolar stress wavefronts are visible as white arcs followed by dark arcs in the Schlieren image (labeled A and B). This single CCD image contains all information needed for the reconstruction of the absorbing shapes (Fig. 3).
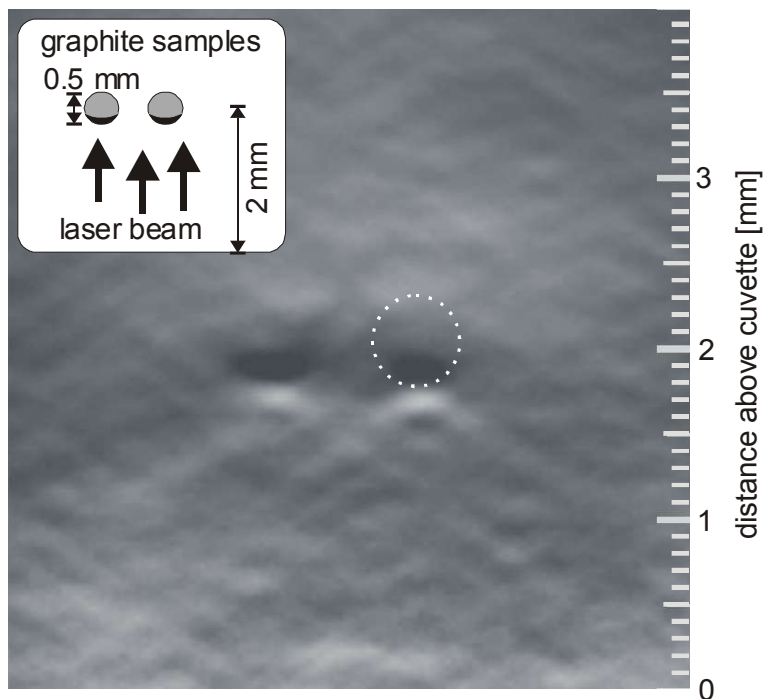
FIG. 3. Real-time reconstruction of two graphite samples (Ø=0.5 mm). The two pencil leads were held perpendicular to the imaging plane, 2 mm above the cuvette. Due to the high light absorption inside the graphite, only the surface of the sample (marked black in the inlet graphic) was heated and therefore generated a pressure transient. The position of one graphite sample is visualized in the image with a white dotted circle. Whereas the dark "half moon" perfectly matches the absorbing volume of the graphite sample, the "white moon" is an artifact caused by the measured bipolar acoustic signal. This single shot image was reconstructed in less than 50 ms without averaging.

times larger than the active Schlieren element size. Therefore, the sensitivity of both methods becomes comparable, if the signal to noise ratio is normalized to the active area of detector. For a clinical use, the excitation pulse energy has to be chosen not to generate irreversible changes in tissue properties. Preliminary in-vivo experiments indicated that small blood vessels can be visualized with an excitation pulse energy of about 1.5 mJ at a wavelength between 500-600 nm. This corresponds to a calculated local temperature rise in the absorbing blood vessel of about 1.5 °C, which is far below the threshold for tissue damage.

The proposed real-time optoacoustic system based on thermoelastic pressure generation operates comparably to medical ultrasound devices. Due to the high spatial resolution, the position of hidden absorbing structures can be determined with an accuracy of about 30 µm, limited by the pulse length of the illuminating flash lamp. The cuvette and the CCD mimic both amplifiers and data storage for every single detector element as required in piezoelectric detector arrays. As all pressure detection principles, the presented Schlieren optical setup is affected by the trade-off between high spatial resolution and high sensitivity. The lack of sensitivity compared to large area piezo electrical sensors can be compensated by using slightly higher laser pulse energies that generate higher pressure transients in the absorbing structures. The main advantage of the Schlieren optical setup is its high spatial resolution and the possibility of on-line diagnostics. The resolution and the contrast of the reconstructed images can further be increased by compensating thermally induced refractive index gradients. This can be done by axial and vertical repositioning of the razorblade. The major advantage compared to still images is that real-time imaging enhances the level of visible detail and moreover allows to monitor dynamic changes.

In summary, Schlieren optical ultrasound detection provides real-time optoacoustic imaging. A high-resolution (in our case, in the range of 30 µm) image can be reconstructed using one single Schlieren exposure. The pulsed OPO (in our case f = 10 Hz) and fast online reconstruction on a PC allow real-time imaging, comparable to medical ultrasound systems.

[1] M. Frenz, G. Paltauf, and H. Schmidt Kloiber, "Laser-generated cavitation in absorbing liquid induced by acoustic diffraction," Physical Review Letters **76** (19), 3546-3549 (1996).

[2] G. Paltauf and H. Schmidt Kloiber, "Measurement of laser-induced acoustic waves with a calibrated optical transducer," Journal of Applied Physics **82** (4), 1525-1531 (1997).

[3] A. A. Oraevsky, S. L. Jacques, and F. K. Tittel, "Measurement of tissue optical properties by time-resolved detection of laser-induced transient stress," Applied Optics **36** (1), 402-415 (1997).

[4] U. Morgner, W. Drexler, F. X. Kartner et al., "Spectroscopic optical coherence tomography," Optics-Letters **25** (2), 111-113 (2000).

[5] C. G. A. Hoelen and F. F. M. de Mul, "Image reconstruction for photoacoustic scanning of tissue structures," Applied Optics **39** (31), 5872-5883 (2000).

[6] A. A. Karabutov, E. V. Savateeva, N. B. Podymova et al., "Backward mode detection of laser-induced wide-band ultrasonic transients with optoacoustic transducer," Journal of Applied Physics **87** (4), 2003-2014 (2000).

[7] P. C. Beard and T. N. Mills, "Extrinsic optical-fiber ultrasound sensor using a thin polymer film as a low-finesse Fabry-Perot interferometer," Applied Optics **35** (4), 663-675 (1996).

[8] K. P. Köstli, M. Frenz, H. P. Weber et al., "Optoacoustic tomography: time-gated measurement of pressure distributions and image reconstruction," Applied Optics **40** (22), 3800-3809 (2001).

[9] G. Paltauf, H. Schmidt Kloiber, K. P. Kostli et al., "Optical method for two-dimensional ultrasonic detection," Applied Physics Letters **75** (8), 1048-1050 (1999).

[10] R. Hooke, *Micrographia: or some physiological descriptions of minute bodies made by magnifying glasses with observations and inquiries thereupon, Observation LVIII*. (Royal Society, London, England, 1665), pp.217-223.

[11] J. R. Meyer-Arendt, *Selected papers on Schlieren optics*. (SPIE Optical Engineering Press, Bellingham, Washington, USA, 1992).

[12] K. P. Köstli, M. Frenz, H. P. Weber et al., presented at the Biomedical Optoacoustics, San Jose, CA, USA, 2000 (unpublished).

Chapter 2

Real-time three-dimensional optoacoustic imaging using an acoustic lens system

Real-time three-dimensional optoacoustic imaging using an acoustic lens system

Abstract

In medical optoacoustics (photoacoustics), absorbing structures, such as blood vessels, hidden inside scattering media are illuminated with short laser pulses resulting in the generation of thermoelastic pressure transients. This initial three-dimensional (3-D) acoustic pressure distribution, which exactly resembles the absorption distribution, was imaged into a water container with a 4f acoustic lens system. An optical darkfield stereo imaging system using a 30 ns flash illumination light was used to capture a snapshot of the pressure-induced refraction index changes in the water container at a predetermined time after the original laser pulse. The imaging system works at 20 Hz frame rate and was designed towards a theoretical resolution of 50 μm. The proposed method directly provides 3-D images of absorbing structures without the need of computational reconstruction algorithms.

Recent interest in optoacoustic imaging,[1-11] which combines high optical contrast and high acoustic penetration depths for biomedical tissue diagnosis, has urged the investigation of various ultrasound detection methods. In optoacoustic imaging, illumination of highly scattering biological tissue with short laser pulses generates pressure transients in absorbing structures by means of thermoelastic effect. An acoustic transducer records these transients at the tissue surface to reconstruct the original absorption distribution. Unlike suitable excitation lasers, which are commercially available, the perfect transducer, a key part of the system, remains to be developed. The ideal acoustic transducer should provide axial and lateral resolution of about 10 μm, high sensitivity in the range of 10 Pa, should be transparent for the exciting laser pulse and should ideally acquire a whole three-dimensional (3-D) absorption distribution at one shot without scanning, preferably at video repetition rates. These requirements partially contradict each other (resolution- sensitivity) or are limited by current technology (3-D acquisition or transparency). Towards this goal many detection methods have been investigated. The limitations i.e. need for scanning, low lateral

resolution, and opaqueness of classical piezoelectric detection[1,4,5,7,9,10] has motivated the development of innovative optical detectors.[2,6,8,11] All these detection methods have in common that the original absorption distribution can only be obtained by image reconstruction, which can be time consuming and may introduce reconstruction artifacts. Another problem are long acquisition times caused by scanning or averaging, which can lead to motion artifacts caused by heartbeat or breathing of the patient.

The system proposed in this letter overcomes some of the limitations by directly performing a 3-D reconstruction of the original pressure distribution inside a water container by means of an acoustic imaging system.[12,13] The acoustically reconstructed image can now be captured by two optical darkfield flash images which provide a stereoscopic projection of the original absorbing structure in real-time.

The setup consisted of a Q-switched Nd:YAG laser source (λ = 1064 nm), which illuminated the scattering sample at a time t = 0 (see Fig. 1). The laser pulses were delivered via a 400 μm fiber equipped with an output lens to produce a 2 mm diameter illumination spot on the sample. The light heated embedded absorbing structures, resulting in an initial 3-D pressure distribution proportional to the locally absorbed energy. An acoustic lens system imaged the initial transient pressure distribution into a water container (see Fig. 2). At t = 65 μs, corresponding to the propagation time of the pressure transients, a 30 ns flash light illuminated the container and a CCD camera acquired two stereoscopic darkfield images from the three dimensional pressure distribution in the container. The image acquisition was running at a repetition rate of 20 Hz synchronized to the Nd:YAG laser. Fig. 2 shows the acoustic lens system consisting of an aspheric aluminum lens covered on both sides with distilled water. The aluminum lens was homemade fabricated on a computer numerical control (CNC) lathe. The dimension of the lens system was chosen in a symmetric 4-f configuration (46 mm water, 22 mm aluminum, 46 mm water) to provide unit magnification both laterally and axially independent of the exact object position. This means that any displacement of the object plane by a distance Δz results in a displacement of the corresponding focused image plane by the same value. The acoustic propagation time from each object plane to the corresponding image plane remains the same, independent of the exact individual object position. Since all acoustic transients originating from multiple object planes are generated simultaneously, all the
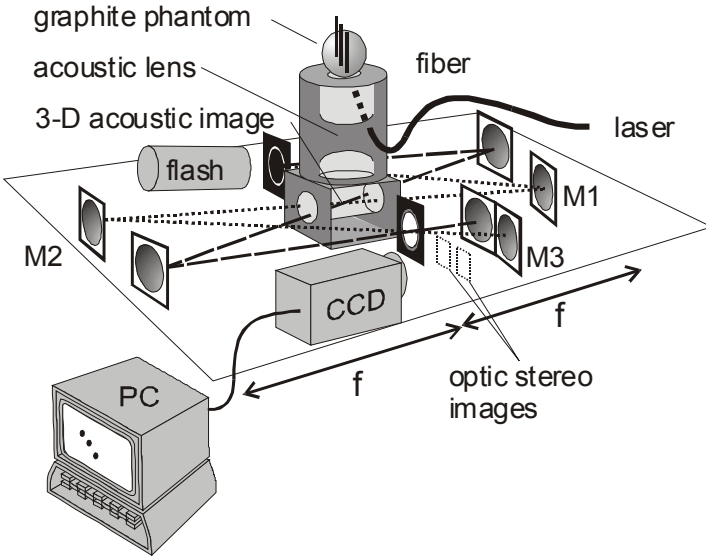
FIG. 1. Optoacoustic imaging setup. The graphite phantom or biological tissue is illuminated with a short laser pulse delivered through a fiber. The generated 3-D transient pressure distribution is imaged with an acoustic lens (details see Fig. 2) into a water container. This 3-D acoustic image is acquired with a stereo dark field optical imaging setup consisting of two optical paths (dashed and dotted) passing the container under an angle of 6º, perpendicular to the acoustical imaging axis. In each path light from the 30 ns flash lamp behind the ring aperture is collimated with a spherical mirror (M1, f = 75 cm), passed through the water container and focused with another mirror (M2, f = 75 cm) onto a circular aperture (d = 14 mm). The ring and the corresponding circular apertures are located in the Fourier planes relative to the object plane to remove the DC component of the image (darkfield). In order to capture both images simultaneously on a single CCD two additional mirrors (M3, f = 30 cm) were used. The stereo images were displayed on a personal computer (PC) monitor where the 3-D effect can be seen using red and green stereo glasses.
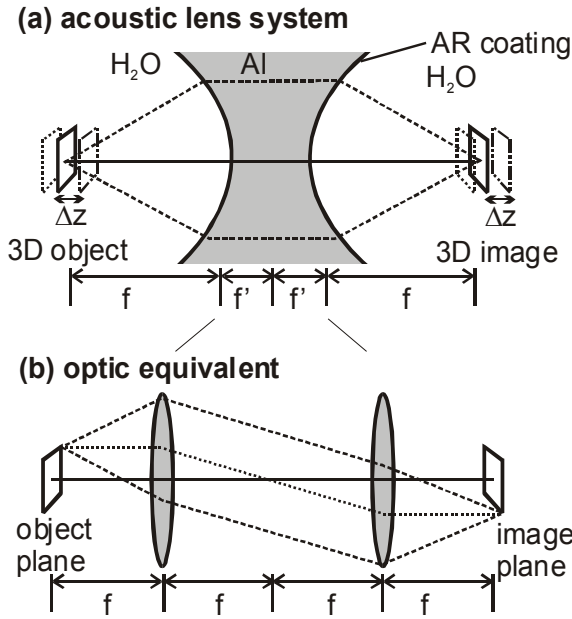
(a) acoustic lens system

FIG. 2. Comparison of acoustic and optic 4-f imaging. The acoustic lens system (a) is arranged in a 4-f configuration. This guarantees axial and lateral unit magnification of the imaged transient pressure distribution. A displacement of the object plane by Δz results in a displacement of the focused image plane by the same value Δz. The low speed of sound compared to the speed of light preserves axial resolution by the propagation time for transient acoustic imaging, which is not possible in (b) the optical equivalent setup. After a time $t = 65$ μs a perfect three-dimensional (3-D) image of the original pressure distribution is formed in the water container behind the lens system. Projections of this 3-D pressure image representing the original absorption distribution was optically visualized with flashed dark field stereo imaging. Acoustic velocity in the aluminum lens is $c_{al} = 6.3$ mm/μs which results in a large relative refraction index of $n = 4.2$ compared to the surrounding water $c_{wa} = 1.5$ mm/μs. Because of the higher acoustic velocity, aluminum acoustic converging lenses are concave not convex like their optical counterparts. To minimize reflection at the water aluminum interface the aspheric surfaces were antireflex coated (AR) with parylene.

corresponding image planes will also be in focus at the same time. This means that the low speed of sound compared to the speed of light preserves axial resolution for transient acoustic imaging, which is not possible in optical imaging. This results in a perfect 3-D pressure image at a fixed time t = 65 μs (acoustic propagation time from one object plane to the corresponding imaging plane). The pressure image is therefore identical to the initial pressure distribution except for small alterations introduced by finite aperture and lens aberrations. The aluminum surfaces were coated with a 40 μm anti reflex (AR) parylene coating to minimize acoustic reflection at the boundary. This broadband AR coating increases the theoretical acoustic intensity transmission of the aluminum lens from 10% to 50% at resonant frequency (13 MHz). The optical imaging setup consisted of a 30 ns flash light, four spherical mirrors (focal length f = 75 cm) arranged in a z-configuration for stereo dark-field imaging under an angle of 6º, two spherical mirrors (focal length f = 30 cm) and a CCD camera with a 50 mm objective for simultaneously acquiring the two stereo images. By inserting a ring aperture and a circular aperture (14 mm diameter) in the Fourier planes,[14] the DC component was removed (dark-field) and the phase variations (pressure modulated refraction index in water) in the container were imaged. Each component of the system was adapted towards a theoretical resolution of 50 μm, determined by the 30 ns flash illumination time, the acoustic attenuation in water and by the acoustic lens aberrations. A computer acquired the single frames from the CCD and displayed them at a repetition rate of 20 Hz on a monitor where the 3-D effect can be seen using red and green stereo glasses. To demonstrate the functionality of the setup, a scattering sample containing several pencil leads was imaged.

Figure 3 shows the result of the 3-D imaging experiment. Five pencil leads with diameter 0.5 mm have been immersed in scattering liquid (μ_s = 0.8 cm^{-1}) and placed above the acoustic lens. The two images acquired simultaneously under an angle of 6º provide a 3-D impression for the human eye. Due to the limitations of the print medium the stereo image pair is showed side by side in Fig. 3a. Fig. 3b shows the optoacoustic image pair of four pencil leads with diameter 0.35 mm immersed in water to demonstrate the 3-D impression without scattering attenuation. No averaging has been performed. The full width half maximum (FWHM) dimensions of the dots in Fig. 3a were estimated to 530 ± 80 μm laterally and 250 ± 34 μm axially. The FWHM dimensions in
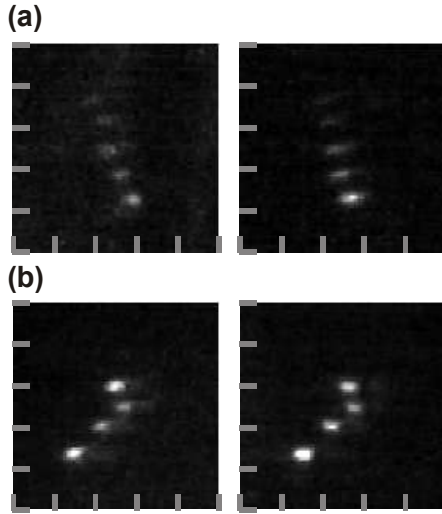
(a)

(b)

FIG. 3. (a) Optoacoustic stereo image pair of five graphite absorbers (diameter = 0.5 mm) immersed in scattering liquid forming a line in space. The lowest dot appears closest (or farthest with converged eyes) and higher points appear successively farther away (or closer with converged eyes). Scattering is attenuating the illumination of the higher dots, which appear fainter and have a less distinct depth. (b) Stereo image of four graphite absorbers (diameter = 0.35 mm) in water, three forming a line and the top one lies behind the others (or in front with converged eyes). These images show that the 3-D effect is perceived independent of the spot brightness, which was not affected by scattering in these images. The images have been acquired with a single 4 mJ illumination laser pulse, no averaging has been performed. The images show a 5 mm x 5 mm area. Hint: To see the 3-D images, focus your eyes as if you were looking at a far away object: this is called "diverging" your eyes. One easy way to do this is to hold the image pair against your nose and very, very slowly pull the images away from your face. Do not focus on the image; let the image come into focus. Be patient, eventually the 3-D image will magically appear.

Fig. 3b were 400 ± 38 µm laterally and 230 ± 38 µm axially. Both lateral dimensions correspond well to the actual pencil lead dimensions of 500 µm in Fig. 3a and 350 µm in Fig. 3b, respectively. The theoretical axial extension of the acoustic disk source on the highly absorbing graphite surface was determined by the length of the laser pulse to about 50 µm. These axial dimensions appear possibly enlarged in the images by surface roughness of the graphite, acoustic lens manufacturing uncertainties or other cumulative broadening effects such as flash light duration. The detection threshold of the system was assessed by illuminating a highly absorbing black tape with constant pulse energy of 1 mJ, but increasing spot size. The minimum radiant exposure still giving a detectable signal in the 3-D image without averaging (SNR = 1) was determined to 1 mJ/cm^2 corresponding to a pressure detection threshold of 0.02 MPa.

In order to optimize the detection system in view of sensitivity and resolution both, the acoustic lens and the optical imaging system need to be optimized. (i) acoustic lens system: Optimization desires a high transmission, i.e. low impedance differences at material boundaries, large refractive index ratios, which means large acoustic velocity differences, and low attenuation for high frequencies. Considering aluminum and plexiglass as possible materials, the theoretical comparison showed that despite low boundary reflections of plexiglass, its high attenuation makes it disadvantageous for frequencies above 10 MHz. Therefore we chose aluminum which additionally features a large acoustic velocity difference to water. The boundary reflections were further reduced by covering the aluminum lens with an antireflex (AR) coating. Also the high acoustic velocity in aluminum gives a high refraction index in water and therefore minimizes lens aberrations. (ii) optical imaging system: A brighter flash illumination can improve the sensitivity up to a level where the optic quality of the glass windows becomes the limiting factor. Because of the high sensitivity each dust particle on the glass windows and inside the container was visible in the dark-field image. Therefore thorough cleaning of the glass windows and high quality water filling were of utmost importance. The optical dark-field setup acts as a projector, integrating a virtual detection volume onto one CCD pixel element. The height and width of the virtual pressure detection volumes correspond to the optical resolution, which is approximately λ/NA (wavelength λ; numerical aperture NA of the optical system). The depth of the volumes corresponds to the depth of sharpness which

is approximately λ/NA^2. For example with visible light ($\lambda = 0.5$ μm) and NA = 0.01 the size of the virtual detector elements becomes approximately 50 μm x 50 μm x 5 mm. This example also shows that the dark field image setup is more sensitive to cylindrical or plane acoustic sources than to point sources because it is integrating over the depth dimension in the water container. By adopting the numerical aperture either the sensitivity or the resolution of the optoacoustic imaging system can be increased. Another consideration is the acquisition of pressure distribution images from many projection angles instead of just a stereo image pair. Combined with tomographic reconstruction this would allow real-time acquisition of the whole 3-D volume using only one exposure avoiding motion artifacts.

In conclusion, a novel real-time 3-D optoacoustic imaging system using an acoustic lens system has been proposed. Absorbing structures hidden in scattering medium can be visualized as stereo images. Therefore the sensitive method is ideally suited to visualize 3-D dynamic tissue changes.

[1] V. G. Andreev, A. A. Karabutov, and A. A. Oraevsky, IEEE Transactions on Ultrasonics, Ferroelectrics and Frequency Control **50** (10), 1383-1390 (2003).

[2] P. C. Beard and T. N. Mills, Applied Optics **35** (4), 663-675 (1996).

[3] M. Frenz, G. Paltauf, and H. Schmidt-Kloiber, Physical Review Letters **76** (19), 3546-3549 (1996).

[4] C. G. A. Hoelen and F. F. M. de Mul, Applied Optics **39** (31), 5872-5883 (2000).

[5] R. G. M. Kolkman, E. Hondebrink, W. Steenbergen, and F. F. M. de-Mul, IEEE Journal of Selected Topics in Quantum Electronics **9** (2), 343-346 (2003).

[6] K. P. Köstli, D. Frauchiger, J. J. Niederhauser, G. Paltauf, H. P. Weber, and M. Frenz, IEEE Journal of Selected Topics in Quantum Electronics **7** (6), 918-923 (2001).

[7] R. A. Kruger, Pingyu-Liu, Yuncai-Fang, and C. R. Appledorn, Medical Physics **22** (10), 1605-1609 (1995).

[8] J. J. Niederhauser, D. Frauchiger, H. P. Weber, and M. Frenz, Applied Physics Letters **81** (4), 571-573 (2002).

[9] J. J. Niederhauser, M. Jaeger, and M. Frenz, Biomedical Optoacoustics IV, Proceedings of the SPIE The International Society for Optical Engineering **4960**, 118-123 (2003).

[10] A. A. Oraevsky, S. L. Jacques, and F. K. Tittel, Applied Optics **36** (1), 402-415 (1997).

[11] G. Paltauf, H. Schmidt-Kloiber, K. P. Kostli, and M. Frenz, Applied Physics Letters **75** (8), 1048-1050 (1999).

[12] L. Bergmann, *Der Ultraschall und seine Anwendung in Wissenschaft und Technik*, 5 ed. (Hirzel, Zürich, 1949).

[13] W. L. Beaver, D. Dameron, and A. Macovski, IEEE Transactions on Sonics and Ultrasonics **SU-24** (4), 235-243 (1977).

[14] G. Serafino and P. Sirotti, Optical Engineering **41** (10), 2549-2555 (2002).

Chapter 3

Transparent ITO coated PVDF transducer for optoacoustic depth profiling

In submission.

Transparent ITO coated PVDF transducer for optoacoustic depth profiling

Abstract

In optoacoustic depth profiling, illumination of scattering biological tissue with short laser pulses generates pressure transients, which are recorded with an acoustic transducer and provide a one dimensional (1D) representation of depth resolved light absorption, a relevant parameter for e.g. transcutaneous medication penetration and portwine stain treatment. We propose a piezoelectric polyvinylidene fluoride (PVDF) transducer with transparent indium tin oxide (ITO) electrodes. With the possibility of laser illumination through the transducer, it is ideally suited for backward optoacoustic detection, a requirement for all parts of the human body not accessible from two sides. The sensitivity of the ITO transducer is comparable to classical aluminum (Al) transducers. Its transparency allows direct placement on the skin and combined with large area homogeneous illumination a 1D acoustic propagation model becomes valid. This eliminates the need for compensation of diffraction effects with deconvolution algorithms. Quantification of the absorption coefficient of a dye sample showed a good convergence toward the real value for large illumination. The proposed transducer is ideally suited for quantifying depth resolved optical properties of layered human skin.

Recently the medical need for highly selective diagnostic methods has motivated research for optoacoustic depth profiling which combines high optical contrast with large acoustic penetration depth.[1-11] In optoacoustics absorbing structures, such as port wine stains, hidden inside scattering media are illuminated with short laser pulses, which generate acoustic transients by means of thermoelastic effect. Acquired with an acoustic transducer, these signals provide quantitative spatial resolved information on optical properties, such as the absorption coefficient, in the tissue. For optoacoustics, most human body parts are not accessible from two sides (forward mode), therefore laser illumination and acoustic sensing needs to be on the same side (backward mode). The commonly used piezoelectric transducers have metal electrodes, which make them opaque for the laser pulse and complicate the optoacoustic transducer design. Many designs have been proposed using ei-

ther a piezoelectric ring for through illumination[4,5,11] or guiding the light around the acoustic transducer.[3,6,8,10] The ring design has a small illumination area making it difficult to illuminate enough light into the tissue without violating the safety limits for laser exposure. The around illumination design requires large distances between the skin and the acoustic transducer leading to lower signal amplitudes and distortion due to acoustic attenuation and diffraction. In both cases acoustic diffraction urge the use of deconvolution algorithms, which complicates direct quantitative measurement. To overcome the opaqueness problem various optical detection methods for optoacoustics have been proposed.[1,2,7,9] However their sensitivity is generally lower than piezoelectric transducer and an additional conversion of the probe light into an electric signal is necessary. We propose a transparent piezoelectric transducer based on indium tin oxide (ITO) coated polyvinilidene flouride (PVDF) which overcomes the limitations mentioned above. ITO is a transparent conductive coating widely used for electrodes in liquid crystal displays (LCD). PVDF is a transparent piezoelectric material ideally suited for sensitive wideband hydrophones. The ITO transducer is compared with a classical aluminum (Al) coated PVDF transducer. The proposed transducer features a high piezoelectric sensitivity, allows quantitative measurement in the acoustic near field directly on the skin and is transparent for the illuminating laser pulse.

As seen in Fig. 1, the experimental setup consisted of two piezoelectric polyvinylidene fluoride (PVDF) transducers, one coated with aluminum (Al) electrodes (a) and one coated with transparent indium tin oxide (ITO) electrodes (b,c). 200 nm of Al was vapour deposited on a 40 μm PVDF for one transducer and 200 nm ITO was sputtered on a 40 μm PVDF foil for the other. A mask was used during the coating of both transducers to have a circular active area of 3 mm diameter. The foils were placed on a 2 cm thick plexiglass (PMMA) backing using glycerin for adhesion by capillary forces. For mechanical protection, a cling film was placed on top using another drop of glycerin for acoustical coupling. A differential amplifier probe connected the piezoelectric electrodes to a digital oscilloscope for data acquisition at a sampling rate of 1 GHz and 15 times averaging. The acoustic transients were generated optoacoustically by illuminating an absorbing layer with short laserpulses. A frequency trebled Nd:YAG laser with an optical parametric oscillator (OPO) generated 5 ns pulses at freely tunable wavelengths of 400-2000 nm. The pulses were coupled into a 600 μm
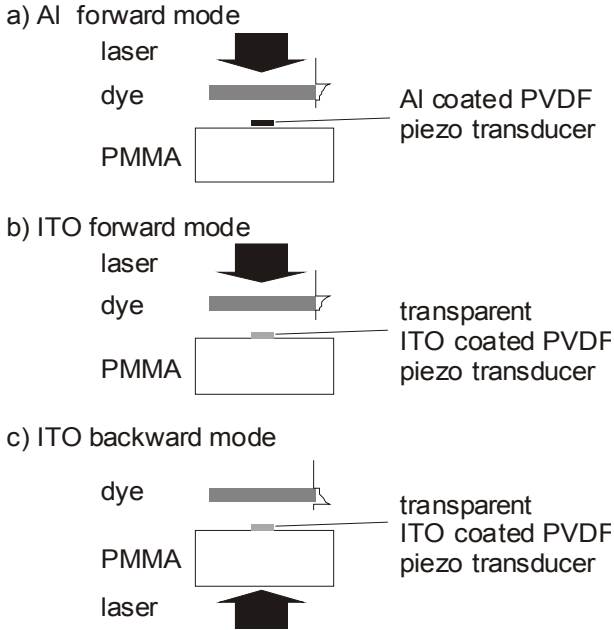
FIG. 1. Experimental setup. The transducers consisted of a piezoelectric PVDF film with either Al electrodes (a) or ITO electrodes (b and c). PMMA was used as a backing material. A 0.8 mm layer of absorbing dye was homogeneously illuminated with a short laserpulse. This generated an acoustic transient representing the light absorption, which was recorded with the transducer. In contrast to Al, ITO is transparent, which allowed illumination not only in forward mode (a and b) but also in backward mode (c). Each configuration was used with two circular laser illumination diameters of 6 mm and 9 mm resulting in a total of six experiments.

fiber and projected on a circular area using a focusing lens on the far end of the fiber. This resulted in homogeneously circular illumination on the sample. For forward measurements the fiber was placed on the opposite side of the absorbing sample relative to the transducer. For backward measurements the fiber was placed behind the plexiglass backing on the same side as the transducer. Backward measurements were only possible with the transparent ITO transducer. Two sets of experiments were conducted: (1) Direct comparison of transducer sensitivity. For direct comparison of sensitivity a 5 mm layer methylene blue solution was placed on either transducer to ensure sufficient absorption in forward mode and therefore eliminate direct transducer irradiation thermal effects. A 15mm diameter spot with 1.8 mJ/cm^2 radiant exposure was chosen to guarantee a 1D acoustic model. (2) Comparison of depth profiling. For the depth profiling a 25 μm Al transducer was used to increase temporal resolution. For the ITO transducer this thickness reduction was not possible because of prototype manufacturing reasons. The absorbing layer consisted of a 300 μM solution of methylene blue in water between two cling films spaced approximately 1 mm apart. It was immersed in water on both sides. The optical absorption coefficient of the dye solution was $\mu_a = 1.65$ mm^{-1} at the wavelength of $\lambda = 577$ nm which was used for the experiment. The absorbing layer was placed in a water bath 2 mm away from the transducer. For comparing the ITO to the aluminum transducer the three possible arrangements (Al forward, ITO forward, ITO backward), each with two illumination diameters 6 mm and 9 mm were investigated, resulting in 6 experiments. The exposure was 4.6 mJ/cm^2 for the 6 mm experiments and 3.9 mJ/cm^2 for the 9 mm experiments, both lying below the safety limit for laser skin irradiation. The thermal background caused by light absorption and heating of the electrodes was acquired by measuring without the absorbing layer and was subtracted from the signals. No other means of reconstruction were used.

For the direct comparison experiment the amplitude of the positive peaks in the signals were compared. The peak amplitudes were 4.0 mV for the Al and 3.75 mV for the ITO transducer. The two materials show similar high piezoelectric sensitivity, which is only slightly affected by the ITO. Fig. 2 shows the results of the 6 depth profiling experiments. The signal of the absorbing layer is clearly visible in all plots between 1.5 and 2.1 μs. With an acoustic velocity of 1.5 mm/μs in water this is equivalent to a thickness of 0.9 mm. As expected from Beer's law,
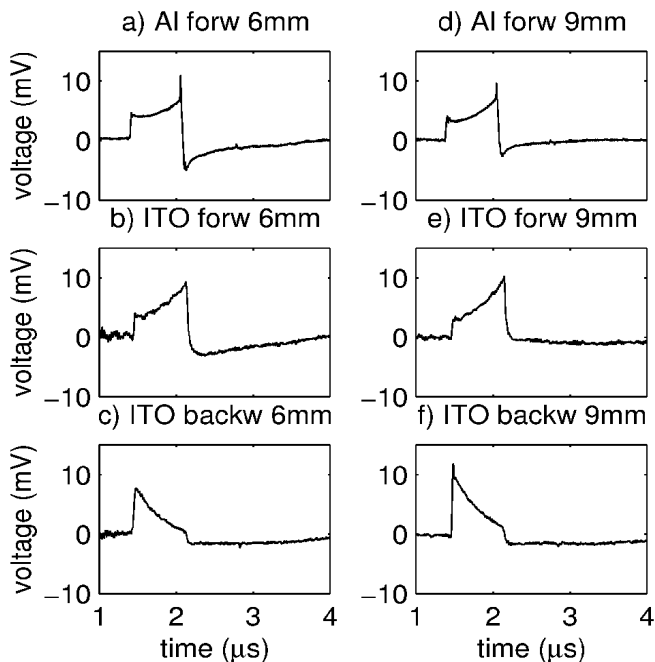
FIG. 2. Experimental results. Subplots (a-c) correspond to the experimental setups (a-c) in Fig. 1 with 6 mm illumination diameter. Subplots (d-f) correspond to the experimental setups (a-c) in Fig. 1 with 9 mm illumination diameter. The six subplots show the exponential slope caused by light absorption inside the dye layer (raise in forward mode and decay in backward mode). In the 6 mm experiments the waveform was distorted by diffraction which is visible as rarefraction periods after the exponential slope. The small peaks at the boundaries of the slopes are caused by higher conversion efficiency in the cling film separating the dye from the surrounding water. Apart from thermal background subtraction and 15 times averaging, no reconstruction, such as deconvolution, has been used.

there is an exponential raise in all the forward measurements and an exponential decay in all the backward measurements caused by light absorption inside the dye. The 6 mm illumination experiments show strong diffraction effects visible as rarefraction minima. With a larger illumination of 9 mm these diffraction effects were reduced. A detail of interest is that in our experiments the Al thermal background of 400 V/m was five times higher than the ITO background of 75 V/m. To quantify the quality of the recorded signals, exponential coefficients were estimated by fitting an exponential function to the data (see Table 1).

The values of table 1 compared to the absorption coefficient of 1.65 mm^{-1} show two characteristics of interest: (1) The exponential coefficients obtained with the Al transducer are too low. This is due to the light reflection at the Al coating causing an overlaid illumination from the opposite side. In our setup two identical arrangements for the ITO and Al transducer were used for comparison but in a sophisticated design a different geometry or covering of the transducer would be necessary (2) The values of the broader 9 mm illumination are closer to the actual value of 1.65 mm^{-1}. Larger illumination area reduces diffraction effects and eliminates the need for correction with deconvolution or calibration techniques. With homogeneous large illumination we can measure a signal undistorted by diffraction if no signal from the illumination boundary can reach the transducer during the measuring period (causality). This is satisfied with the following condition: illumination radius > transducer radius + sensing depth. In our case with an illumination radius of 4.5 mm and a transducer radius of 1.5 mm the condition was satisfied until a depth of 3 mm, which corresponds to the far end of the dye sample. Nevertheless there are small deviations in the exponential coefficient, which can be explained by finite input properties of the differential amplifier or nonhomogeneous illumination artifacts. The capacitance of the transducer and the input resistance of the differential probe act as a high pass filter. This explains the negative deviation of the estimated coefficients from the true values for the 9 mm cases. This signal distortion can be corrected using frequency compensation filtering. Another effect is caused by the connection resistance and the differential amplifier input capacitance, which mimic a low pass filter. For Al this resistance was in the low Ω range, but for the ITO this resistance varied from 100-10000 Ω depending on the sputtering process. This resulted in lower cuttoff frequencies and loss

	6 mm illum	9 mm illum
Al forward	0.68 mm^{-1}	1.06 mm^{-1}
ITO forward	1.15 mm^{-1}	1.32 mm^{-1}
ITO backward	-2.40 mm^{-1}	-1.94 mm^{-1}

TABLE 1. Exponential fit to the data to show the influence of illumination area. The table shows the exponential coefficients obtained by fitting an exponential function to the corresponding traces in Fig. 2 in the time interval between 1.55 µs and 2.0 µs. For the ITO forward and backward measurements the coefficients converge towards the actual absorption coefficient of 1.65 mm^{-1} for larger illumination (9 mm). The low Al coefficients are caused by backreflected light from the Al electrodes overlaying an exponential contribution in reverse direction. The ITO values show that good quantification of optical parameters without deconvolution of diffraction effects is possible for large area illumination. The small systematic negative deviation of the values are primarily caused by finite amplifier input resistance and can therefore be compensated. For large homogeneous illumination, the theoretical 1D acoustic propagation model becomes valid.

of high frequency features in the ITO depth profiles. For the depth profiling experiments the ITO transducer thickness was not reduced to avoid deformation caused by mechanical stresses induced by the non-optimized ITO sputtering process. With an optimized process it should be easy to fabricate thinner transducers featuring a larger bandwidth. Transducers with 25 μm or even 9 μm thickness would allow detailed investigation of skin features or medication penetration with theoretical depth resolutions of up to 6 μm. A major advantage of the design is that, due to the transparent ITO, the transducer can be directly placed on the surface of the sample under investigation. This facilitates compliance with the above illumination condition to allow direct 1-D depth sensing without diffraction distortion.

We propose a transparent ITO coated PVDF transducer for optoacoustic 1D depth sensing. While having a similar sensitivity compared to an Al coated transducer, it is 5 times less susceptible to thermal signals caused by light absorption in the electrodes and provides transparency for the illuminating laser beam in backward mode. Its utility was demonstrated on a known absorbing dye layer. The estimated absorption coefficients converged well towards the real value for large illumination. Therefore the proposed transducer design is ideally suited for quantitative measurement of depth resolved optical properties of layered structures in the human skin.

[1] P. C. Beard and T. N. Mills, "Extrinsic optical-fiber ultrasound sensor using a thin polymer film as a low-finesse Fabry-Perot interferometer," Applied Optics **35** (4), 663-675 (1996).

[2] J. D. Hamilton, T. Buma, M. Spisar et al., "High frequency optoacoustic arrays using etalon detection," IEEE Transactions on Ultrasonics, Ferroelectrics and Frequency Control **47** (1), 160-169 (2000).

[3] A. A. Karabutov, E. V. Savateeva, N. B. Podymova et al., "Backward mode detection of laser-induced wide-band ultrasonic transients with optoacoustic transducer," Journal of Applied Physics **87** (4), 2003-2014 (2000).

[4] K. P. Koestli, M. Frenz, H. P. Weber et al., "Pulsed optoacoustic tomography of soft tissue with a piezoelectric ring sensor," Proceedings of the SPIE The International Society for Optical Engineering **3916**,

67-74 (2000).

[5] R. G. M. Kolkman, E. Hondebrink, W. Steenbergen et al., "In vivo photoacoustic imaging of blood vessels using an extreme-narrow aperture sensor," IEEE Journal of Selected Topics in Quantum Electronics **9** (2), 343-346 (2003).

[6] R. A. Kruger, Pingyu-Liu, Yuncai-Fang et al., "Photoacoustic ultrasound (PAUS)-reconstruction tomography," Medical Physics **22** (10), 1605-1609 (1995).

[7] J. J. Niederhauser, D. Frauchiger, H. P. Weber et al., "Real-time optoacoustic imaging using a Schlieren transducer," Applied Physics Letters **81** (4), 571-573 (2002).

[8] J. J. Niederhauser, M. Jaeger, and M. Frenz, "Comparision of laser-induced and classical ultrasound," Proceedings of the SPIE The International Society for Optical Engineering **4960**, 118-123 (2003).

[9] G. Paltauf, H. Schmidt-Kloiber, K. P. Kostli et al., "Optical method for two-dimensional ultrasonic detection," Applied Physics Letters **75** (8), 1048-1050 (1999).

[10] J. A. Viator, B. Choi, M. Ambrose et al., "In vivo port-wine stain depth determination with a photoacoustic probe," Applied Optics **42** (16), 3215-3224 (2003).

[11] M. Yamazaki, T. Shimada, S. Sato et al., "Characteristics of a photoacoustic detector for biomedical measurements," Review of Laser Engineering **30** (10), 598-601 (2002).

Part II

Medical ultrasound combined with optoacoustics for real-time imaging *in vivo*

Chapter 4

Comparison of laser-induced and classical ultrasound

Comparison of laser-induced and classical ultrasound

Abstract

A classical medical ultrasound system was combined with a pulsed laser source to allow laser-induced ultrasound imaging (optoacoustics). Classical ultrasound is based on reflection and scattering of an incident acoustic pulse at internal tissue structures. Laser-induced ultrasound is generated *in situ* by heating optical absorbing structures, such as blood vessels, with a 5 ns laser pulse (few degrees or fraction of degree), which generates pressure transients. Laser-induced ultrasound probes optical properties and therefore provides much higher contrast and complementary information compared to classical ultrasound. An ultrasound array transducer in combination with a commercial medical imaging system was used to record acoustic transients of both methods. Veins and arteries in a human forearm were identified *in vivo* using classical color doppler and oxygenation dependent optical absorption at 660 nm and 1064 nm laser wavelength. Safety limits of both methods were explored. Laser-induced ultrasound seems well suited to improve classical ultrasound imaging of subcutaneous regions.

1 Introduction

Medical ultrasound imaging is widely used as a diagnostic tool. The demand for better images has motivated the development of additional ultrasound imaging modes such as second harmonic imaging or color doppler. Laser-induced ultrasound also known as optoacoustics or photoacoustics[1, 2, 3, 4, 5, 6] is a novel technique of ultrasound imaging which has the potential to provide higher contrast and functional information of subcutaneous structures. Because laser-induced ultrasound is based on optical properties of the tissue, it is complementary to conventional ultrasound.

This paper compares side by side classical and laser-induced ultrasound imaging. For the laser-induced ultrasound images a ns laser pulse was used to generate an ultrasound wave instead of using the transmitted ultrasound pulse. Otherwise an identical medical ultrasound system was used for imaging. It has, however, to be mentioned that the detection system used was far from optimum for the laser-induced ultrasound due to

the limited bandwidth of the array transducer and the image reconstruction algorithm which was optimized for a classical ultrasound system.

Classical ultrasound is based on reflection and scattering of ultrasonic pulses. Imaging depth depends on acoustic frequency and extends to tens of centimeters in human tissue. A blood vessel can be identified on a ultrasound image by its reflecting boundary and absence of scattering inside the vessel (See Fig. 1). In contrast, laser-induced ultrasonic imaging shows the interior of a blood vessel. Optical absorption of blood varies with wavelength and strongly depends on the oxygenation level. By combining images taken at multiple wavelengths, various structures, such as veins or arteries, can be distinguished (Fig. 2). In comparison to tens of centimeters for classical ultrasound, the laser-induced ultrasonic imaging depth is limited to a few centimeters by optical absorption and scattering.

In vivo experiments comparing the imaging of blood vessels in a human forearm show that complementary information can be extracted using the two modes.

2 Safety considerations

Before clinically using laser-induced imaging thorough safety considerations should be made. In our case we need to comply with both, ultrasound and laser safety limits.

In the USA, ultrasound safety limits were designed with medical ultrasound devices in mind and are therefore difficult to relate to the laser-induced case. According to the National Electrical Manufacturer Association (NEMA) ultrasound devices should display thermal index (TI) and mechanical index (MI)[7, 8]. These measurements correspond to temperature increase and mechanical damage caused by the ultrasound. The new ultrasound safety guides in Germany and England provide an easier approach[9, 10]. They limit the acoustical stress to 4 MPa (40 bar) and the temperature rise to 4 K (for 15 minutes sessions).

Skin laser irradiation safety-levels are defined by ANSI Standard Z136.1 (1993) [11]. For 10 ns pulses and wavelengths of 400-700 nm the maximal permissible exposure (MPE) is 20 mJ/cm^2. For near infrared the MPE raises exponentially to 100 mJ/cm^2 at wavelengths above 1050 nm.
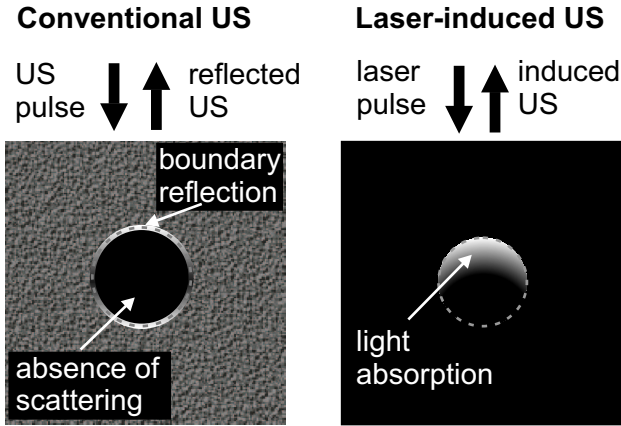
Figure 1: Schematic images of blood-vessels (dashed circles) using classical and laser-induced ultrasound. The blood-vessel appears in a conventional ultrasonic B-scan image (left picture) as a black circle with white boundaries. The dark area corresponds to an absence of acoustic scatterers (blood is acoustically homogenous). In laser-induced ultrasound imaging, a laser pulse at i.e. 660 nm is absorbed by the blood inside the vessel. This leads to an exponentially distributed instantaneous heating, which generates the ultrasonic pulse. Large blood vessels are therefore visible as "half moons" on laser-induced ultrasonic images (right picture). Smaller blood vessels (compared to the optical penetration depth in blood) may appear homogenously illuminated. (US = ultrasound)
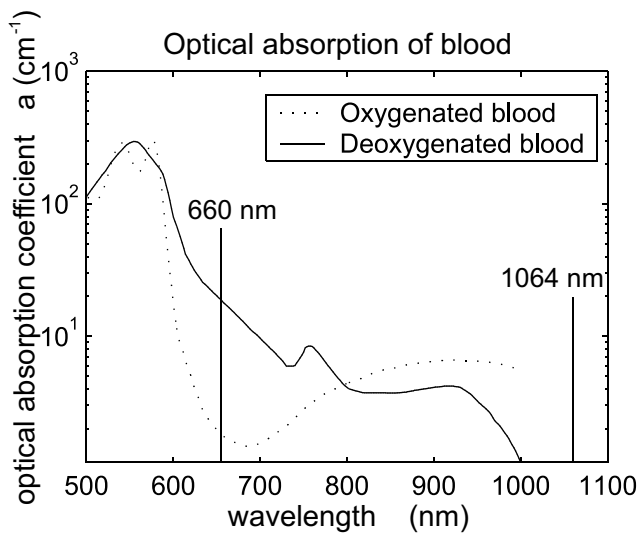
Figure 2: Optical absorption spectrum of blood. The spectrum shows the oxygen dependent absorption at the two wavelengths used for imaging (spectrum from http://omlc.ogi.edu/).

In most cases laser MPE compliance provides also ultrasound safety compliance.

3   Materials and Methods

A classical ultrasound system (Kontron Sigma 330) with a 7.5 MHz linear array transducer, was used for the experiments. The system provides conventional B-Mode and color doppler imaging. For the laser-induced images the transmitting ultrasound pulse was suppressed and a 5 ns laser pulse was triggered instead. The laser source was a frequency tripled Quantel Brilliant B Nd:YAG laser with a GWU 400-2600 nm tunable optical parametric oscillator (OPO). During ultrasound recording, dynamic focusing and time gain compensation were kept identical for classical and laser-induced imaging. The only difference was the temporal compression of the sequences by a factor of two for the laser-induced case to fit the half acoustic travelling distance.

The laser pulse of the OPO was split into two identical pulses by a beamsplitter cube and coupled each to a 600 μm core fiber. To obtain almost homogeneous illumination of the tissue sample, the two fibers were connected at their distal end to a PMMA waveguide. One waveguide was placed on either side of the array transducer, as shown in Fig. 3, resulting in two illumination spots of 4 mm x 2 mm. With the combined spot area of 16 mm^2 the energy limit is 16 mJ at $\lambda = 1064$ nm (MPE 100 mJ/cm^2). The *in vivo* images (Fig. 5) were taken with pulse energies E = 10 mJ, which is far below the safety limit. A translation stage moved the fibers along the waveguides to get fully illuminated scans.

In order to verify the imaging setup, two pencil leads ($\varnothing = 0.5$ mm) forming a cross were stuck into a beef steak. This sample was imaged using the classical and the laser-induced ultrasonic mode. In addition, the authors left forearm 8 cm from the wrist on the thumb side was imaged *in vivo* using both methods.
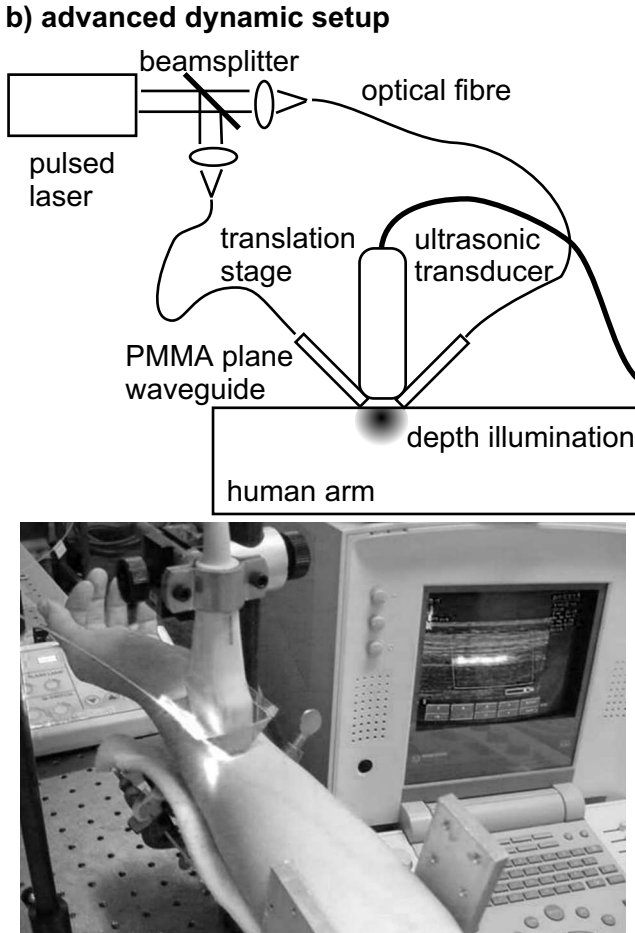
Figure 3: Imaging setup. An optical parametric oscillator generated pulses at freely tunable wavelengths of 400-2600 nm. Two 600 μm fibers were used to deliver the light through a PMMA plane guide into the human arm (on the setup picture on the right, only one fibre is visible). The fibers were moved with a translation stage to scan over 3 cm imaging width. The illumination spot sizes were chosen to comply with the maximal permissible exposure on the skin.
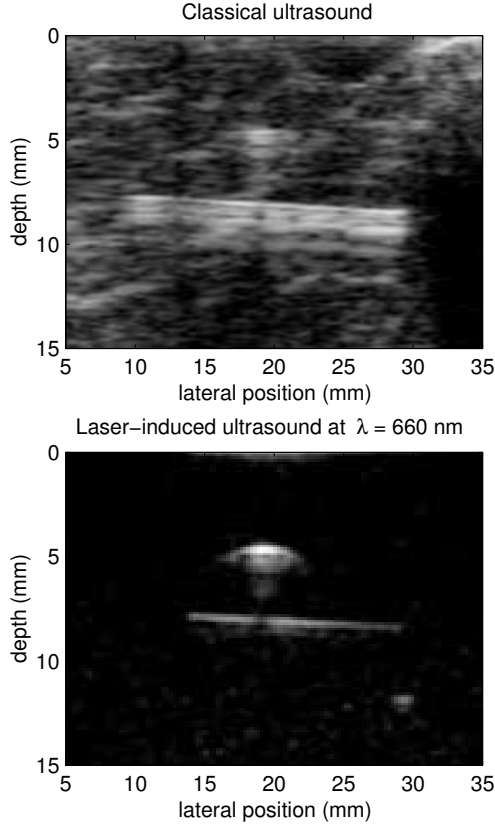
Figure 4: Classical and laser-induced images of a beefsteak containing two crossed 0.5 mm pencil leads. One pencil lead is oriented parallel to the imaging plane at 8 mm depth the other perpendicular to it at 5 mm depth. The laser illumination spot diameter was 1 cm (lateral position 15 mm to 25 mm) and the pulse energy was 8 mJ at a wavelength of 660 nm. The brightness is proportional to the signal intensities in both picture. Both images were reconstructed the same way. Because of the strong optical absorption, the pencil leads show superior contrast on the laser-induced image compared to the conventional ultrasound image. In both images the pencil lead at 5 mm depth produced shading on the lower pencil lead. No averaging was applied.

4   Results

Fig. 4 shows images of two crossed pencil leads ($\varnothing = 0.5$ mm) embedded in a beefsteak obtained width both techniques. The classical ultrasound image shows strong scattering but lower contrast. The broad image of the deeper lying lead is caused by internal reflections of the ultrasound wave. In comparison, the laser induced image, despite the limited transducer bandwidth, gives an image of high contrast. The image reveals that light at a wavelength of 660 nm penetrates tens of mm deep into this highly scattering biological tissue. The reconstruction of both images were done using an identical algorithm provided by the commercial ultrasound system.

In Fig. 5 the left forearm 8 cm away from the wrist is imaged using both methods. The two main blood vessels were identified as an artery and a vein by color doppler imaging. The venous flow however, was made only visible by ligation of the arm and applying pressure on the hand. Both vessels are clearly visible in the conventional ultrasonic image (a). The vessel contour lines are finer in the laser-induced images and show slightly higher contrast compared with the conventional image. This complies with the theoretical higher contrast and resolution. In the 660 nm laser-induced ultrasonic image (b), the contour of the vein is more distinct than of the artery. In the 1064 nm image (c), the artery is more pronounced. This agrees with the absorption spectrum of blood, which shows a strong absorption of deoxygenated blood at 660 nm and a strong absorption of oxygenated blood at 1064 nm. The large vessels are visible in both techniques, however laser-induced ultrasound allows distinction of the two blood vessels without ligation and manipulation of the arm.

Furthermore, the laser-induced ultrasound pictures give a more detailed image of the subsurface area above the vein. Both images reveal absorbing structures, which are more pronounced in the 660 nm image than in the 1064 nm image. This corresponds to the vascular system anatomy, which predicts small veins in the subsurface layers. Unfortunately these structures cannot be further investigated with the current setup due to the limited resolution of the 7.5 MHz array transducer.

Another though negative detail in the laser-induced image are surface or ghost echoes. They are caused by pressure transients generated by light
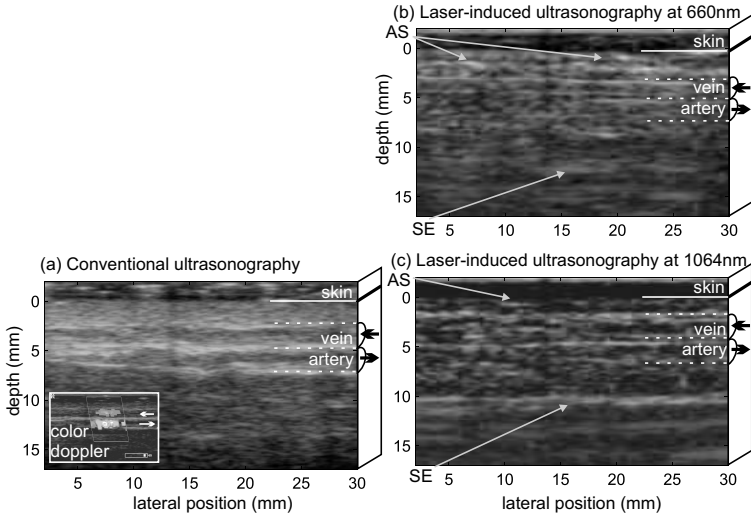
Figure 5: *In vivo* imaging comparison of forearm. A vein (depth 4 mm) and an artery (depth 6 mm) are imaged using (a) Conventional ultrasound (b) Laser-induced ultrasound; optical wavelength λ = 660 nm; pulse energy E=2.2 mJ (c) Laser-induced ultrasound; λ = 1064 nm; E=9.6 mJ. The two main blood vessels were identified using color doppler (see inlet image) and are visible on all the images. The vein and the artery can be identified on the laser-induced ultrasound images by their oxygen dependent signal. SE denotes an echo signal which originally was generated by absorption of the initial laser pulse in the melanin at the tissue surface and reflected at the blood vessel (appears at double distance because of the double acoustic path). AS denotes absorbing structures between the skin and the vein in (b) and (c). This layer is known to contain small veins, whose absorption should generate strong signals at 660nm. The resolution of these structures, which are not visible in (a), was bandwidth limited by the 7.5 MHz linear array transducer. No averaging was applied.

absorption at the skin (i.e. melanin) or transducer surface, which propagate like classical ultrasound pulses into the tissue and echo off blood vessels. Because of their return trip they appear in doubled depth compared to the laser-induced signals. At large depths the ghost echo signals become predominant and could therefore complicate or even depth limit laser-induced imaging in reflection mode. This limitation motivates the combination of the two techniques in a single system that covers both, large ultrasound depths and high resolution laser-induced functional imaging for shallow regions.

5   Conclusions

Laser-induced *in vivo* images have been acquired in combination with a classical ultrasound system. Safety limits of such a combined system have been discussed. Side by side comparison of the images showed the specific advantages and disadvantages of the two complementary methods. A combination of the two techniques in a single system represents a novel diagnostic tool for dermatology offering a subtly differentiated picture of the vascular system of the skin.

6   Acknowledgements

References

[1] M. Frenz, G. Paltauf, and H. Schmidt Kloiber, "Laser-generated cavitation in absorbing liquid induced by acoustic diffraction," *Physical Review Letters* **76**(19), pp. 3546–9, 1996.

[2] A. A. Oraevsky, S. L. Jacques, and F. K. Tittel, "Measurement of tissue optical properties by time-resolved detection of laser-induced transient stress," *Applied Optics* **36**(1), pp. 402–15, 1997.

[3] G. Paltauf and H. Schmidt Kloiber, "Measurement of laser-induced acoustic waves with a calibrated optical transducer," *Journal of Applied Physics* **82**(4), pp. 1525–31, 1997.

[4] A. A. Karabutov, E. V. Savateeva, N. B. Podymova, and A. A. Oraevsky, "Backward mode detection of laser-induced wide-band ultrasonic transients with optoacoustic transducer," *Journal of Applied Physics* **87**(4), pp. 2003–14, 2000.

[5] K. P. Kostli, D. Frauchiger, J. J. Niederhauser, G. Paltauf, H. P. Weber, and M. Frenz, "Optoacoustic imaging using a three-dimensional reconstruction algorithm," *IEEE Journal of Selected Topics in Quantum Electronics* **7**(6), pp. 918–23, 2001.

[6] J. J. Niederhauser, D. Frauchiger, H. P. Weber, and M. Frenz, "Real-time optoacoustic imaging using a schlieren transducer," *Applied Physics Letters* **81**(4), pp. 571–3, 2002.

[7] NEMA, *Standard for Real Time Display of Thermal and Mechanical Acoustic Output Indices on Diagnostic Ultrasound Equipment*, no. UD 3-1998, National Electrical Manufacturers Association, Rosslyn, VA, USA, 1998.

[8] FDA, *Information for Manufacturers Seeking Marketing Clearance of Diagnostic Ultrasound Systems and Transducers*, U.S. Department of Health and Human Services, Food and Drug Administration, Center for Devices and Radiological Health, http://www.fda.gov/cdrh/ode/ulstran.pdf, 1997.

[9] GEFAU, *Ultrasound Field Safety Classification for Medical Diagnostic Devices*, no. GEFAU N 01, Gesellschaft für andgewandte Ultraschallforschung, Duisburg, Germany, 2001.

[10] NPL, *Measurement Good Practice Guide: Recomended ultrasound Field Safety Classification for Medical Diagnostic Devices*, no. 50, National Physical Laboratory, Teddington, Middlesex, United Kingdom, 2001.

[11] ANSI, *Safe Use of Lasers*, no. Z136.1(1993), American National Standards Institute, New York, USA, 1993.

Chapter 5

Classical and laser-induced ultrasonography: a comparative study

In submission.

Classical and laser-induced ultrasonography: a comparative study

Abstract

In laser-induced ultrasonography human tissue is illuminated with short (5 ns) laser pulses. Absorbing structures, such as blood-vessels, inside the tissue are heated and generate an ultrasonic wave by virtue of the thermoelastic effect. The ultrasound wave was recorded using a commercial medical ultrasound device and an image of the absorbing structures was reconstructed. Targeting structures to a depth of a few centimeter, laser-induced ultrasonography supplies superior contrast and higher spatial resolution compared to conventional ultrasonography. Using multiple laser wavelengths (660nm and 1064nm) for irradiation of human blood vessels, the laser-induced method allows the ultrasound device to "see" color and therefore estimate spatially resolved blood oxygenation levels. Targeting different depths and tissue characteristics, the two methods are complementary and can be ideally combined in a single medical diagnostic device to improve conventional ultrasound.

1 Introduction

During the last decades, medical ultrasonography became a widely established medical diagnostic tool. The increasing demand for high contrast and more informative images led to the development of new ultrasound imaging modes, such as color doppler and three dimensional imaging. Although, a major limitation of conventional ultrasonography is the weak contrast of the images, in some cases contrast enhancing media can be used. This drawback has recently stimulated research in combining conventional ultrasound with high contrast optical methods targeting at better cancer or vascular and dermal pathology diagnosis. Apart from providing magnitudes higher contrast, optical methods have the advantage of probing wavelength dependent features, such as blood oxygenation. Laser-induced ultrasonography is such a combination which allows ultrasound devices to "see" color and visualize fine blood vessels in the skin tissue with high contrast.

In laser-induced ultrasonography, also known as optoacoustics or pho-
toacoustics [1–7], highly scattering biological tissue is illuminated with a
short laser pulse. The laser pulse heats (only few degrees or fractions of
a degree) absorbing structures hidden inside the tissue resulting in exci-
tation of a pressure- or ultrasonic wave (thermoelastic effect). By detect-
ing the ultrasound on the surface with a conventional array transducer,
absorbing structures can be imaged. Using multiple wavelengths of illu-
mination pulses, the absorption spectrum or "color" of the structures can
be determined. This allows, compared with the known blood absorption
spectrum, to estimate spacial resolved blood oxygenation levels inside the
tissue. Laser-induced ultrasonography is therefore ideally suited for func-
tional imaging of small blood vessels up to a depth of a few centimeters.

Laser-induced ultrasonography overcomes limitations of other opti-
cal medical imaging techniques, such as optical coherence tomography
(OCT) [8] or optical tomography (OT). Optical scattering is limiting high
resolution OCT to imaging depths of few millimeters, which is one order
of magnitude lower than the few centimeters achievable by laser-induced
ultrasonography. Although OT reaches depths of few centimeters, its spa-
tial resolution is almost completely lost due to optical scattering. The
achievable spatial resolution of laser-induced ultrasonography does not
depend on optical scattering and is therefore comparable or slightly higher
than conventional ultrasonography (sub millimeter resolution).

Most of the laser-induced ultrasonography research has focused on
theoretical work [5], phantoms [6] and one dimensional detection [2, 4].
The few published *in-vivo* imaging studies often required impractical scan-
ning of the transducer and the images are hard to relate to actual physio-
logical structures [9].

This paper overcomes these technical limitations and presents an hu-
man *in vivo* imaging comparison of laser-induced and classical ultrasound
on a single device. The advantages and limitations of both methods are
compared and discussed aiming at a combination of the two methods in a
high quality imaging device.

2 Materials and Methods

2.1 Basics of laser-induced and conventional ultrasound

To compare conventional and laser-induced ultrasonography the mechanisms can be considered as a three step process. 1) The energy transport into the tissue (sound or light). 2) The reflection or conversion of energy inside the tissue. 3) The transport of information from the targeted structure to the tissue surface. Table 1 summarizes the processes and limitations of the two methods.

Common for both, the conventional and laser-induced ultrasonic imaging is, that acoustic waves carrying the information are measured on the surface of biological tissue. The difference of both methods is the way the acoustic waves are generated. To compare the imaging capabilities of the two methods theoretical contrast, resolution and imaging depths were compared.

The contrast of conventional ultrasonography is based on acoustic impedance mismatch between different biological materials. Homogenous materials, such as blood, do not produce an echo signal and can therefore not be imaged. Inhomogeneous tissues or boundaries do by virtue of impedance mismatch at the boudaries, produce an echo signal. The acoustic impedances (Z) of soft biological tissue are in the small range of $1.35 \cdot 10^6$ (fat) and $1.65 \cdot 10^6$ (muscle) kg/m^{2}s. This results in an intensity reflection factor $r = |\frac{Z_1 - Z_2}{Z_1 + Z_2}|^2$ of only 0.01. However, the contrast of laser-induced ultrasonography depends on variations of the optical absorption coefficients (μ_a) of the tissue, which can be two orders of magnitude in the visual spectrum. The generated initial pressure $p = \Gamma \cdot \mu_a \cdot H$, Γ being the Grüneisencoefficient (≈ 0.2 for 37°C water) and H being the radiant exposure, is proportional to the optical absorption coefficient. The optical absorption coefficients of soft biological tissue are in the range of 0.1 (dermis) and 10 (blood) cm^{-1} for a wavelength of 650-1000 nm. This is a contrast factor of 100 which is far superior to conventional ultrasonography.

The imaging resolution is in both cases limited by the acoustic attenuation α of the tissue which is approximately proportional to the frequency f in the 1-50 Mhz range. Meaning the longer the travelling distance of a acoustic wave, the less high frequency content is available. This re-

Physical process	conventional ultrasonography	laser-induced ultrasonography
step 1: energy transport into the tissue	type of energy	
	sound	light
	transport effects	
	attenuation (α/f=1 $\frac{dB}{cmMhz}$) scattering negligible	absorption (μ_a=0.1 cm^{-1}) scattering (μ'_s=10 cm^{-1})
	penetration depth	
	limited by attenuation (10 cm)	limited by scattering (1 cm)
step 2: energy conversion inside the tissue	type of conversion	
	reflection	thermoelastic effect
	conversion efficiency depends on	
	acoustic impedance difference $r = \lvert\frac{Z_1-Z_2}{Z_1+Z_2}\rvert^2$ ($r = 0.01$)	Grüneisencoefficient and absorption $p = \Gamma \cdot \mu_a \cdot H$ ($\Gamma = 0.2$)
step 3: energy transport to the tissue surface	type of energy	
	sound	sound
	transport effects	
	attenuation (α/f=1 $\frac{dB}{cmMhz}$) scattering negligible	attenuation (α/f=1 $\frac{dB}{cmMhz}$) scattering negligible
	penetration depth	
	limited by attenuation (10 cm)	limited by attenuation (10 cm)

Table 1: Theoretical comparison of conventional and laser-induced ultrasonography. The values in parenthesis are typical values for biological tissue at 37°C in the 1-50 MHz acoustic range and in the near infrared (650-1000 nm) optical range.

sults in a lower spatial imaging resolution for larger depths. The optical resolution, which is limited by the wavelength, is orders of magnitude higher than the acoustic resolution. Therefore the imaging resolution of the laser-induced ultrasonography is limited by the acoustic attenuation. For a certain imaging depth, the acoustic travelling path for conventional ultrasonography is twice as long as for laser-induced ultrasonography. Therefore a doubled resolution is expected for the laser-induced method given the laser pulse is short enough.

The maximal imaging depth of conventional ultrasonography, which is limited by acoustic attenuation and reflection, is typically about 20 cm. The imaging depth of laser-induced ultrasonography is limited by the optical penetration depth of light into tissue. The effective light extinction coefficient $\mu_{eff} = \sqrt{3\mu_a(\mu_a + \mu'_s)}$ (diffusion approximation), with reduced scattering coefficient μ'_s and absorption coefficient μ_a, is about 1 cm^{-1} for human skin tissue at near infrared wavelengths. This results in an imaging depth in the few cm range for laser-induced ultrasonography.

Because of the fundamental differences between the laser-induced and conventional ultrasound, the images contain complementary information about the biological tissue. B-Mode ultrasound visualizes acoustic inhomogeneities, whereas laser-induced ultrasound monitors light absorption. Fig. 1 shows how a blood vessel is being imaged with both methods.

Of interest are the functional imaging capabilities of the two methods. Conventional ultrasonography can be supported by color doppler imaging [10, 11]. This technique uses the doppler effect to visualize movements like blood flow inside the tissue, which enhances the visibility of blood vessels and allows the distinction between arteries and veins based on flow direction. Doppler techniques, however, have difficulties visualizing small veins because of the slow blood flow and the small flow volume, which results in small doppler signals.

Laser-induced ultrasonography provides the possibility to choose the optimum illumination wavelength. Similar to pulse oximetry where two wavelengths are used to estimate the blood oxygenation level, a spatially resolved oxygenation image can be acquired with laser-induced ultrasonography. At a wavelength of 660 nm the deoxygenated blood has a higher absorption coefficient than oxygenated blood (See Fig. 2), whereas at 1064 nm the absorption of deoxygenated blood is lower. Using these two wave-
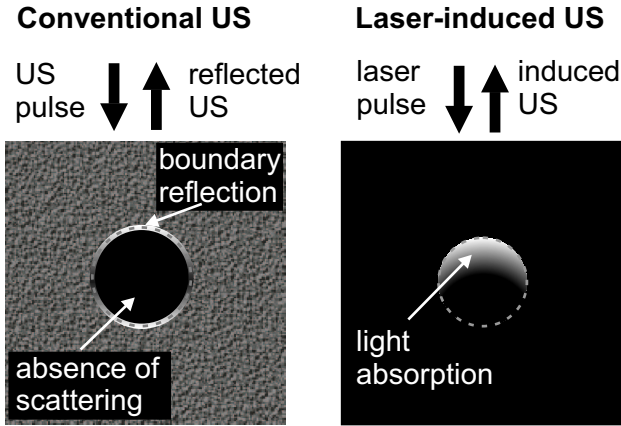
Figure 1: Imaging of blood-vessels (dashed circles) using conventional and laser-induced ultrasonography. US = ultrasound. The blood-vessel appears in the ultrasonic B-scan image as a black circle with white boundaries. The dark area corresponds to an absence of acoustic scatterers (acoustic homogenous blood). The boundaries reflect the ultrasound. In laser-induced ultrasound imaging, the laser pulsed is mainly absorbed by the blood inside the vessel. This leads to an exponentially distributed instantaneous heating, which generates the ultrasonic pulse. Depending on the absorption depth to vessel diameter ratio, blood vessels are either generate "half moons" (λ=590 nm) or whole disks (NIR wavelengths) pressure signals.
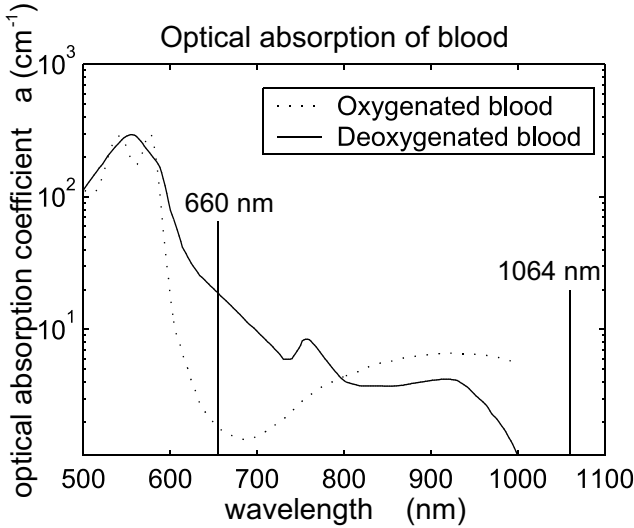
Figure 2: Optical blood absorption spectrum of fully oxygenated and de-oxygenated blood. The optical penetration depth in biological tissue is high in the 650 nm - 1000 nm near infrared range because of the low absorption. At 660 nm wavelength, deoxygenated blood absorption is higher than the oxygenated absorption. At 940 nm the oxygenated blood absorption has a local maximum and is higher than deoxygenated blood. Absorbtion measurement at two wavelengths can determine the oxygenation level. The blood spectra are taken from http://omlc.ogi.edu/.

lengths, arteries with high oxygenated blood and veins with deoxygenated blood can be distinguished in the image. As this functional imaging does not depend on blood flow, even small arterial blood-vessels can be imaged and identified with laser-induced ultrasonography [7].

2.2 Setup

All the ultrasound images have been acquired with a Sigma 330 medical ultrasound system manufactured by Kontron Medical AG, Basel, Switzerland. The Sigma 330 includes B-Mode imaging and color doppler mode. We used a 7.5 LVS linear 79 element array transducer with a total width of 37.92 mm. Therefore the array elements had a spacing of 0.48 mm.

The transducer had a bandwidth of 4 - 12 MHz.

The Sigma 330 allows time gain compensation (TGC) and dynamic focusing with an analog beamforming stage during recording of the ultrasonic signals. The beamforming stage sums the signal from 2 to 16 neighboring elements with appropriate delays before digitizing the signal. The number of elements are chosen such that the aperture of the receiver is a factor of 2.5 smaller than the focusing distance. The TGC and beamformer use predefined sequences that were factory optimized for medical imaging quality.

The excitation of the laser-induced ultrasonography was performed with a Brilliant B Q-switched frequency tripled Nd:YAG laser manufactured by Quantel S.A, France, pumping an Optical Parametric Oscillator manufactured by GWU-Lasertechnik, Germany. The laser system generated 6 ns laser-pulses of selectable wavelength (450-2000 nm) with an energy of up to 15 mJ at a repetition rate of 10 Hz. In addition, the Nd:YAG fundamental 1064 nm wavelength was directly used for illumination if a higher radiant exposure was necessary.

For the conventional ultrasound images the Sigma 330 was used without modifications. For the laser-induced ultrasound images, the ultrasound pulse generator was disabled and the Brilliant laser was fired instead. Since the laser-induced ultrasonic waves are generated directly by the targeted tissue structure, they travel the distance between tissue structure and surface only once, which was compensated by compressing the TGC and the beamforming sequences of the Sigma 330 by a factor of two.

In the simple static setup, the 1 cm diameter laser beam was focused with a 40 mm cylindric lens to allow the illumination of the tissue just below the 45° tilted ultrasonic transducer. See Fig. 3a.

In the advanced dynamic setup (see Fig. 3b), the laser beam was delivered through two 600 μm fibres. The fibres were scanned with a IXE-C-T translation stage, manufactured by Phythron, Germany, to allow a wider imaging range. Two PMMA plane waveguides were used to obtain a defined illumination area on the skin. The dimensions were chosen to comply with the laser safety limits for maximal permissible skin exposure (ANSI Z136.1-1993).
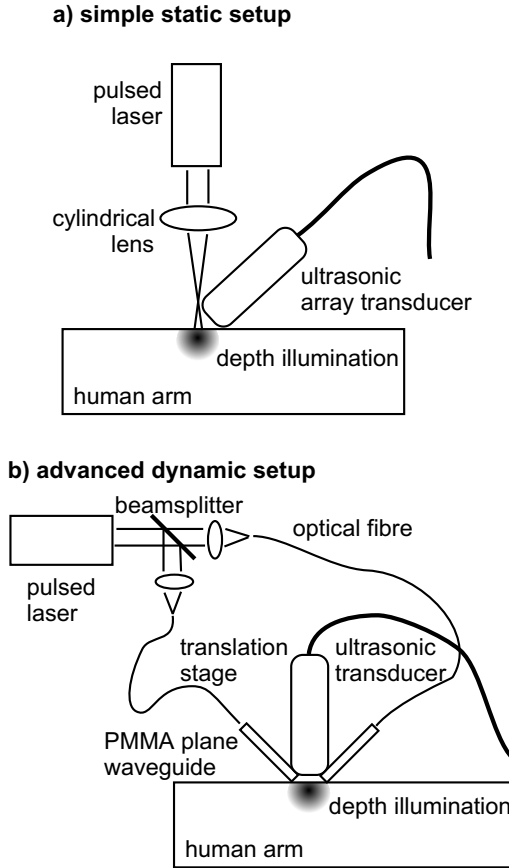
Figure 3: Imaging setups. (a) In the simple static setup a cylindrical lens was used to illuminate a static spot area on the skin. The laser pulses propagated trough the 1cm x 2mm spot area into the tissue and induced ultrasonic transients inside blood-vessels. (b) In the advanced dynamic setup two $600\,\mu$m fibres were used to deliver the light through a PMMA plane guide into the human arm. The fibers were moved with a translation stage to scan over 3 cm imaging area. The illumination spot sizes were chosen to comply with the maximal permissible exposure on the skin.

2.3 Experiment

To validate the experimental setup we imaged a known sample with conventional and laser-induced ultrasonography. A beefsteak containing 3 highly light absorbing pencil leads was placed on the transducer of the simple static setup. The pencil position in images acquired with conventional ultrasonography and laser-induced ultrasonography were compared. Pencil leads should give a strong signal for both methods because of their high acoustic impedance and the high optical absorption.

After validation of the experiment, the blood vessels of the forearm of an human volunteer were imaged in vivo using conventional and laser-induced (advanced dynamic setup) ultrasonography. The flow was visualized on the Sigma 330 using color doppler imaging to identify the blood vessels. For the laser-induced ultrasonography the laser was tuned to 660 nm and 1064nm to be able to differentiate between oxygenated and de-oxygenated blood (see Fig. 2), and to have deep optical penetration into the tissue. The different absorption spectra were used for identifying arteries and veins. To compare the imaging contrast of the two methods and to estimate the image quality improvement by temporal averaging, a cross-section through the forearm 10 cm from the wrist was imaged using both methods (Fig. 6).

3 Results

As shown in Fig. 4, the black graphite leads, embedded in a beefsteak, generated strong laser-induced signals. The optical contrast is magnitudes higher compared to conventional ultrasonography due to the strong absorption in the black graphite. The position match on both images confirm a correct reconstruction for both methods.

In Fig. 5 the left forearm 8 cm away from the wrist was imaged using both methods. The two main blood vessels were identified as an artery and a vein by color doppler imaging. The venous flow was only made visible by ligation of the arm and applying pressure on the hand. These two vessels are clearly visible in the conventional ultrasonic image (see Fig. 5a). The vessel contour lines are finer in the laser-induced images and show slightly higher contrast compared with the conventional image.
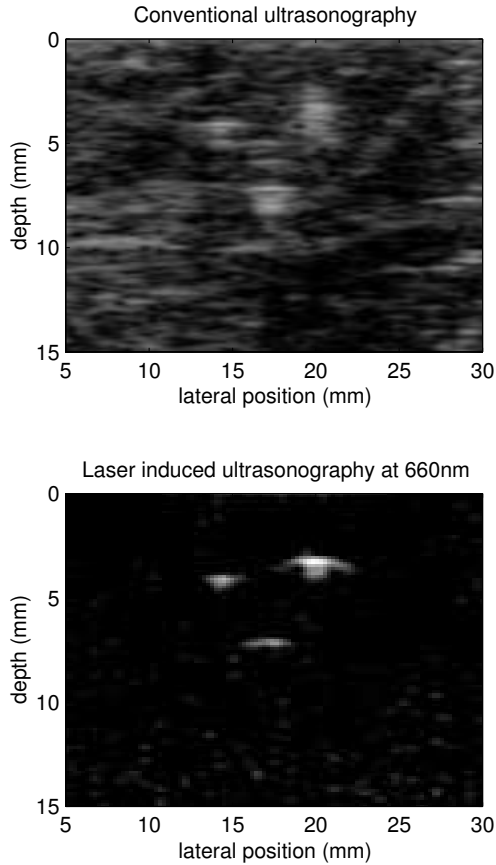
Figure 4: Experimental setup validation. Conventional and laser-induced images of a beefsteak containing three pencil leads (bright spots in the images). brightness is proportional to the signal intensities in both picture. Identical receiver settings were used to acquire these unaveraged images. Because of the strong optical absorption, the pencil leads show superior contrast on the laser-induced image compared to the conventional ultrasound image. The positions of the samples match on both images.

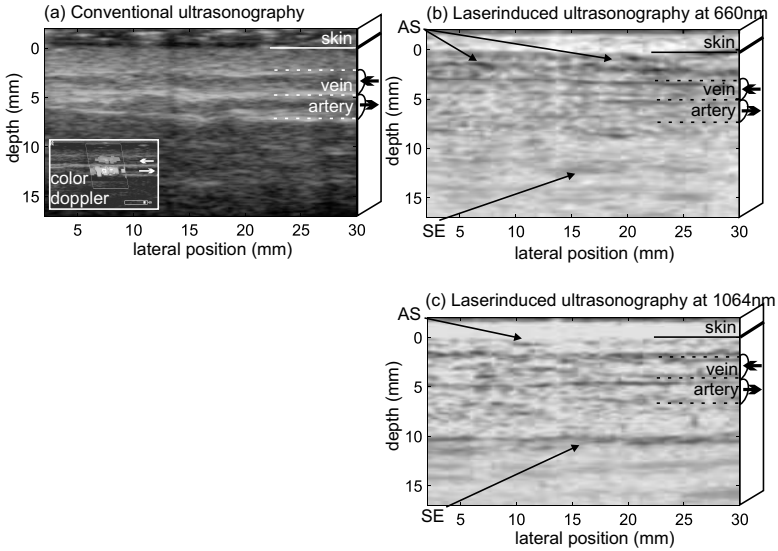Figure 5: Invivo imaging comparison of forearm. A vein (depth 4 mm) and an artery (depth 6 mm) are imaged using (a) Conventional ultrasound (b) Laser-induced ultrasound; optical wavelength $\lambda = 660$ nm; pulse energy E=2.2 mJ (c) Laser-induced ultrasound; $\lambda = 1064$ nm; E=9.6 mJ. The two main blood vessels were identified using color doppler (see inlet image) and are visible on all the images. SE denotes surface echo, which is the surface optoacoustic pulse reflected at the blood vessel (appears at double distance because of the double acoustic path). AS denotes absorbing structures between the skin and the vein in (b) and (c). This layer is known to contain small veins, whose absorption should generate strong signals at 660nm. The resolution of these structures, which are not visible in (a), was bandwidth limited by the 7.5 MHz transducer. In the laser-induced images high amplitudes correspond to dark pixels, in the ultrasound images high amplitudes correspond to bright pixels. No averaging was performed.

This complies with the theoretical higher contrast and resolution. In the 660 nm laser-induced ultrasonic image (b), the contour of the vein is more distinct than of the artery. In the 1024 nm image (c), the artery is more pronounced. This corresponds to the absorption spectrum of blood, which suggest strong absorption of deoxygenated blood at 660nm and a strong absorption of oxygenated blood at 1024nm. The two blood vessels can therefore be distinguished based on their oxygenation level.

In the conventional ultrasonic image, the layer between the vein and the skin surface looks undifferentiated. The laser-induced images of these layers reveal absorbing structures, which are more pronounced in the 660 nm image than in the 1024 nm. This would correspond with the vascular system anatomy, which predicts small veins in those subsurface layers. Unfortunately these structures cannot be further investigated with the current setup due to the limited resolution of the 7.5 MHz transducer used.

Fig. 6 shows a cross-section through a blood-vessel pair in a human forearm. The lateral position of the large blood vessel (at depth 7 mm) match with both techniques. Due to tissue compression artifacts (several minutes interval between the ultrasound and the laser-induced image) the large vessels appear in a slightly different depth on the two modes. In addition to the large blood vessel, the laser-induced images show detailed structures (at depth 4 mm) with high contrast, which are faintly visible on the classical ultrasound image but are harder to distinguish from background speckling. Only four times temporal averaging of the laser-induced images resulted in superior quality compared to non-averaged images.

4 Discussion

The two methods target on different imaging depths. While conventional ultrasound imaging mainly focuses on the 1-10 cm range, laser-induced ultrasonic imaging rather focuses on the 1-10 mm range. The conventional ultrasonic images in the 1 cm range are blurry because of the low contrast. The comparison is somehow unbalanced because we are comparing a sophisticated conventional ultrasound device, optimized for imaging, with a fundamental research setup. Laser-induced ultrasonographic resolution was limited by the 7.5 MHz transducer and the laser energy was limited
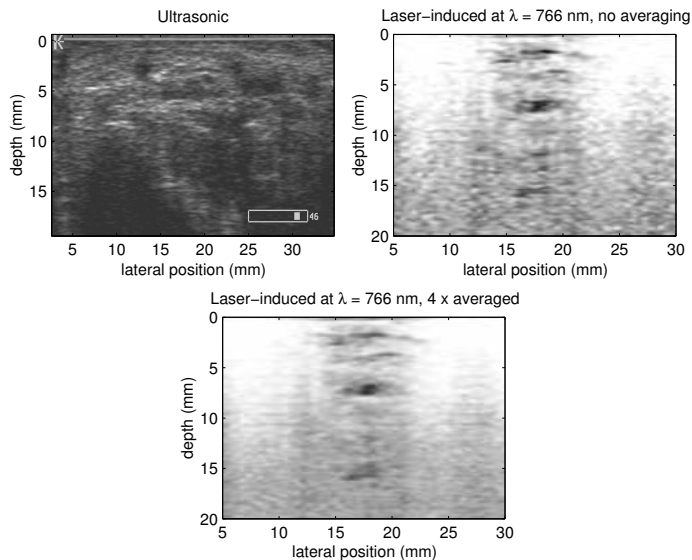
Figure 6: Temporal averaging. The plots show a cross-section through blood-vessel (artery/vein pair) in a human forearm. The conventional ultrasound image (not averaged) is shown along with two laser-induced images, one was not averaged and one was 4 x temporal averaged. The temporal averaging increases image quality. The laser-induced images were acquired with the static setup and a pulse energy of E=6.5 mJ at 766 nm. The tissue was illuminated using the simple setup between 13 mm and 22 mm, therefore the regions outside this area show the system noise-floor without any signal. In the laser-induced images high amplitudes correspond to dark pixels, in the ultrasound images high amplitudes correspond to bright pixels.

by our laser system. Even thought the laser-induced ultrasonography is far from being well-engineered, the comparison could reveal some fundamental differences of the two methods.

The main advantages of laser-induced ultrasound in the 1 cm range are enhanced visibility of small blood vessels and functional imaging based on absorption spectra. Venous blood vessels are well visible because of high absorption. In contrast to color doppler no additional treatment (ligation, active pressure) is necessary to visualize even small veins. For large arteries, color doppler is superior to laser-induced imaging.

The classical ultrasound image quality can be improved using contrast agents, which increase the ultrasound signal of blood. In laser-induced ultrasound blood produces large ultrasound signals without any additional means, due to its large absorption coefficient. However there is also the possibility of using exogenous optical contrast agents, such as selectively binding antigens with absorbing nano gold-particles, to enhance the contrast of cancerous tissue.

Laser-induced imaging is ideally suited for dermatological skin characterization because it allows in vivo visualization of small absorbing structures in the skin. The blood supply of transplanted tissue or melanomas could be investigated for diagnostic purposes. The visibility of small blood vessels and blood oxygenation levels could also provide new possibilities for angiology diagnostics.

Laser-induced ultrasonic imaging is a save method, because it uses non ionizing irradiation at save levels. The laser irradiation levels used were below the maximal permissible skin exposure defined by ANSI standards. The pulse energies for the imaging were limited by our laser equipment and could be further increase to get better quality images without violating the standards.

To gain further improvement of the laser-induced ultrasonic images, the transducer bandwidth should be increased and the ultrasound device must be modified to provide realtime imaging. This would allow to adopt imaging parameters online and would greatly enhance the visual quality of the images

5   Conclusion

Laser-induced ultrasound provides high contrast functional imaging on a conventional ultrasound device. Targeting on the centimeter range, laser-induced ultrasonography is predestined to extend the capabilities of conventional ultrasound devices for small blood vessel monitoring. The combination of the two complementary methods in a single device could create a new generation of high contrast online imaging systems.

6   Acknowledgements

References

[1] M. Frenz, G. Paltauf, and H. Schmidt Kloiber, "Laser-generated cavitation in absorbing liquid induced by acoustic diffraction," *Physical Review Letters*, vol. 76, no. 19, pp. 3546–9, 1996.

[2] A. A. Oraevsky, S. L. Jacques, and F. K. Tittel, "Measurement of tissue optical properties by time-resolved detection of laser-induced transient stress," *Applied Optics*, vol. 36, no. 1, pp. 402–15, 1997.

[3] G. Paltauf and H. Schmidt Kloiber, "Measurement of laser-induced acoustic waves with a calibrated optical transducer," *Journal of Applied Physics*, vol. 82, no. 4, pp. 1525–31, 1997.

[4] A. A. Karabutov, E. V. Savateeva, N. B. Podymova, and A. A. Oraevsky, "Backward mode detection of laser-induced wide-band ultrasonic transients with optoacoustic transducer," *Journal of Applied Physics*, vol. 87, no. 4, pp. 2003–14, 2000.

[5] K. P. Kostli, D. Frauchiger, J. J. Niederhauser, G. Paltauf, H. P. Weber, and M. Frenz, "Optoacoustic imaging using a three-dimensional

reconstruction algorithm," *IEEE Journal of Selected Topics in Quantum Electronics*, vol. 7, no. 6, pp. 918–23, 2001.

[6] J. J. Niederhauser, D. Frauchiger, H. P. Weber, and M. Frenz, "Real-time optoacoustic imaging using a schlieren transducer," *Applied Physics Letters*, vol. 81, no. 4, pp. 571–3, 2002.

[7] J. J. Niederhauser, M. Jaeger, and M. Frenz, "Comparison of laser-induced and classical ultrasound," in *Proc. SPIE*, vol. 4960, Bellingham, WA, 2003.

[8] U. Morgner, W. Drexler, F. X. Kartner, X. D. Li, C. Pitris, E. P. Ippen, and J. G. Fujimoto, "Spectroscopic optical coherence tomography," *Optics-Letters*, vol. 25, no. 2, pp. 111–13, 2000.

[9] A. A. Oraevsky, E. V. Savateeva, S. V. Solomatin, A. A. Karabutov, V. G. Andreev, Z. Gatalica, T. Khamapirad, and P. M. Henrichs, "Optoacoustic imaging of blood for visualization and diagnostics of breast cancer," in *Proc. SPIE*, vol. 4618, Bellingham, WA, 2002, pp. 81–94.

[10] D. F. Switzer and N. C. Nanda, "Doppler color flow mapping," *Ultrasound in Medicine and Biology*, vol. 11, no. 3, pp. 403–16, 1985.

[11] G. R. Curry and D. N. White, "Color coded ultrasonic differential velocity arterial scanner (echo flow)," *Ultrasound in Medicine & Biology*, vol. 4, no. 1, pp. 27–35.

Chapter 6

Novel real-time optoacoustic system for *in vivo* high contrast vascular imaging

Novel real-time optoacoustic system for *in-vivo* high contrast vascular imaging

Abstract

In optoacoustic imaging, short laser pulses irradiate highly scattering human tissue and adiabatically heat embedded absorbing structures, such as blood vessels, to generate ultrasound transients by means of the thermoelastic effect. We present an optoacoustic vascular imaging system that records these transients on the skin surface with an ultrasound transducer array and displays the images online. With a single laser pulse a complete optoacoustic B-mode image can be acquired. The optoacoustic system exploits the high intrinsic optical contrast of blood and provides high contrast images without the need of contrast agents. The high spatial resolution is determined by the acoustic propagation and is only limited to the submillimeter range by our 7.5 MHz linear array transducer. A Q-switched alexandrite laser emits save, non-ionizing short laser-pulses at a wavelength of 760 nm, which allows an imaging depth of a few centimeters. The system provides real-time images at frame-rates of 7.5 Hz and optionally displays the classically generated ultrasound image alongside the optoacoustic image. The functionality of the system was demonstrated *in-vivo* on human finger, arm and leg. The proposed system combines the merits and most compelling features of optics and ultrasound in a single high contrast vascular imaging device.

1 Introduction

The medical need for high quality images from inside the human body has motivated research on optoacoustic imaging [1–14], a new imaging technique, which merges high optical contrast with large acoustic penetration depths. In optoacoustics, highly scattering human tissue is illuminated with short laser pulses. The laser pulses heat (degrees or fraction of degrees) absorbing structures, such as blood vessels, resulting in acoustic pressure transients. These acoustic transients propagate to the tissue surface and are recorded with ultrasound transducers. The recorded signals contain spatially resolved information on optical tissue properties.

Starting in the late 90ties, biomedical optoacoustic research focused on the development of suitable detectors and reconstruction algorithms [1–8]. Only few *in-vivo* imaging studies have been presented so far [9–12]. In all these studies the images were reconstructed off-line.

From medical imaging devices in clinical use today, ultrasound is one of the most cost-effective and easy to use technique. The real-time capability of ultrasound imaging simplifies the search for crucial diagnostic locations and enhances visibility of important image details. However the low contrast of ultrasound demands the use of contrast agents or extensive training of the investigator to correctly interpret the images.

We propose an optoacoustic device, combining a pulsed laser source with a conventional ultrasound system, which provides real-time (7.5 frames per second) high contrast images of absorbing tissue structures. To demonstrate its functionality we image small subcutaneous blood vessels of a human volunteer *in-vivo* in real-time. The appropriate imaging locations were easily found because of the online image reconstruction capability and the high image contrast. For comparison, classical ultrasound images were displayed alongside the optoacoustic images. The research aims at a combination of the two highly complementary techniques into a single device valuable for diagnosis.

2   Theory

Optoacoustic pressure transient generation in biological tissue is based on the thermoelastic effect. The initial pressure distribution caused by a short laser pulse is $p_0(x, y, z) = \Gamma \cdot \mu_a(x, y, z)H(x, y, z)$, with initial pressure p_0, unitless Grüneisencoefficient Γ, absorption coefficient μ_a and radiant exposure H.

The initial pressure is proportional to the absorption coefficient μ_a, which is a wavelength dependent optical tissue property. Different chromophores have their specific optical absorption spectra. By scanning the illumination laser wavelength, different absorbers such as oxygenated or deoxygenated hemoglobin, water or melanin can be distinguished according to their spectrum. Optoacoustic imaging can therefore display functional information such as blood oxygenation level by irradiating at multiple laser wavelengths.

The local radiant exposure H depends on the optical absorption and scattering properties of the tissue. H can be approximated by diffusion theory because scattering is the predominant effect in biological tissue. Assuming homogenous optical properties, the effective attenuation coefficient becomes $\mu_{eff} = \sqrt{3\mu_a(\mu_a + \mu'_s)}$ (absorption coefficient μ_a and reduced scattering coefficient μ'_s). If highly scattering tissue is illuminated with a pencil beam, scattering spreads the beam inside the tissue into a large cone-shaped volume. This behavior combined with the maximal permissible exposure for skin motivates broad area illumination on the skin to achieve maximum exposure of deep structures.

Optoacoustic imaging can not use focused illumination inside the tissue, a technique known from classical ultrasound imaging, because of strong optical scattering. The focusing in classical ultrasound is necessary because the received ultrasound signal is based on the weakly back reflected or scattered portion of the direct ultrasound. In optoacoustics, however, the ultrasound is generated directly inside the tissue by the tissue structure of interest and the forward portion of the ultrasound reaching the transducer is recorded. This signal is mainly undistorted by acoustic scattering or reflection and allows high-resolution reconstruction of the initial distributed transient ultrasound sources. In optoacoustics, in contrast to optical tomography, optical scattering is even an advantage as it improves illumination homogeneity (less shadowing). The light only serves to provide high imaging contrast but the high spatial resolution is completely given by the acoustic propagation. Optoacoustics therefore combines the merits and most compelling features of optics and acoustics.

3   Materials and Methods

A Q-switched alexandrite laser (Storz Medical) provides laser pulses for optoacoustic ultrasound generation. The pulses had the following properties: pulsewidth $\tau=60$ ns, pulse-energy E up to 50 mJ and wavelength $\lambda=760$ nm. The pulses were coupled into a 400 μm fiber and delivered to the optical illumination system of the ultrasound transducer. As seen in Fig. 1, the illumination system consisted of a lens, a prism and two mirrors, to guide the light around the transducer and image the distal fiber core onto the skin surface. This produced a homogenous circular illumi-

nation spot on the skin with a diameter of 25 mm corresponding to an area of about 5 cm^2.

For optoacoustic imaging, the illuminating light penetrates into the highly scattering skin and gets absorbed in absorbing structures, such as blood vessels or melanin layer. The associated local temperature increase (fraction of degrees) generates an acoustic stress transient by means of thermoelastic effect. Due to the high speed of light the initial ultrasound transients of different absorbing structures are generated almost simultaneously. They exactly image the absorbed energy distribution. The ultrasound transients propagate to the skin surface where they are recorded using an ultrasound transducer.

Two 1 cm thick transparent ultrasound coupling pads (by Geistlich Pharma AG, Switzerland) were placed between the skin and the linear array ultrasound transducer (by Vermon S.A, France), which had a mid frequency of 7.5 MHz, a bandwidth of 70% and an element pitch of 0.4 mm. An aluminum coated 8 μm plastic foil, which did not influence the acoustic propagation, was placed between the coupling pads and the transducer to shield off backscattered laser irradiation on the transducer and therefore reduce generation of acoustic signals on the transducer surface. The ultrasound transients, measured on 64 channels of the transducer simultaneously, were acquired with a Digital Phased Array Ultrasound System (DiPhAS) by Fraunhofer Institute for Biomedical Engineering, St. Ingbert, Germany. The system allows parallel data acquisition of all transducer elements. The DiPhAS acquired data at 30 MHz sampling rate and transferred these data in real-time via a fast connection to a pentium processor. 64 channels with 1024 Samples and 16 bit resolution were transferred for every optoacoustic image. One single excitation laser pulse was enough to acquire a complete optoacoustic image.

The image reconstruction was done in a dual processor 1000 MHz intel pentium computer. The fourier reconstruction algorithm by Köstli et al. [3] was slightly extended and applied to the data. The following notation was used: lateral dimension x, depth dimension y, corresponding k-vectors k_x and k_y, time t, corresponding angular frequency ω and sound velocity c. The reconstruction was conducted in the following steps: (1) Zero padding of the original 64x1024 matrix to reduce frequency quantization artifacts. (2) 64x2048 2D-FFT from (x,t) space to (x,ω) space. (3)
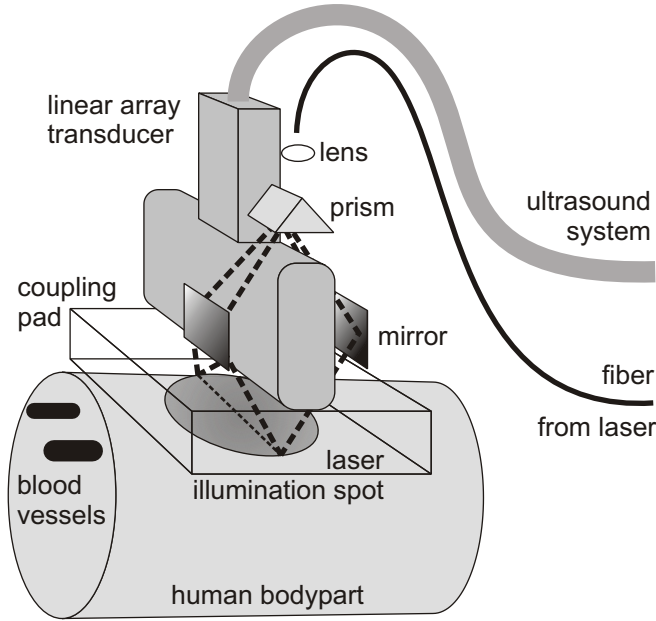
Figure 1: Combined optoacoustic and ultrasound real-time imaging setup. Short laser pulses are delivered through a fiber to the illumination system consisting of a lens, a prism and two mirrors. The illumination system images the core of the fiber around the transducer onto a homogeneously illuminated spot on the skin. The light penetrates into the highly scattering tissue and is absorbed in blood vessels resulting in ultrasound transient generation (thermoelastic effect). The ultrasound transients propagate back to the skin surface, through the transparent acoustic coupling pad onto the ultrasound transducer. The signals of 64 transducer elements are simultaneously recorded with an ultrasound system and passed onto a computer. The computer reconstructs an absorption distribution image and displays it on a screen with a repetition rate of 7.5 Hz. One single laser pulse is enough to get a complete image on the screen in less than 100 ms reconstruction time. Classical echo ultrasound images can also be acquired for side by side comparison or for mixed mode imaging.

Rearrangement and weighting of the matrix values from the (k_x, ω) space to the (k_x, k_y) space according to the relation $\omega^2 = c^2(k_x^2 + k_y^2)$ and reducing the matrix to 64x512. Only the positive k_y half was filled. (4) 64x512 inverse 2D-FFT from (k_x, k_y) space to (x, y) space. (5) Taking the absolute of the complex output values.

The reconstructed images were weighted with depth illumination compensation and mapped onto 256 gray scale values. A hardware accelerated graphic card and OpenGL were used to interpolate and display the images on the computer screen in real-time. The setup runs at 7.5 Hz repetition rate given by the used laser. For side by side comparison classical ultrasound-echography images could be acquired in alternation with the optoacoustic images.

To demonstrate the applicability of the system we imaged the subcutaneous blood vessels in the wrist, the arm and the leg of a human volunteer. To assure laser safety we kept the exposure and average power well below the ANSI-Z136.1 limit of 20 mJ/cm^2 and 0.2 W/cm^2 respectively. With the flexible fiber delivery the whole transducer was movable and could be easily placed on any body part.

4 Results

The *in-vivo* optoacoustic image of the index finger (Fig. 2) shows small blood vessels with high optical contrast. In the ultrasound image the echo signal from the bone is predominant. The comparison shows that the two techniques extract complementary information. The finger is usually not investigated with 7.5 MHz ultrasound system because of lacking contrast and resolution. However the high optical contrast of optoacoustics gives detailed images of these regions using identical ultrasound equipment.

Fig. 3 shows *in-vivo* images of a blood vessel in the leg taken in a cross and longitudinal section. The blood vessel is well visible at the same depth below skin in all four images. The real-time feature of the system allowed online finding and investigation of the correct imaging planes. The comparison of the two techniques shows that they extract complementary information.

Fig. 4 shows a movie sequence of a branching blood vessel in a human forearm taken with *in-vivo* optoacoustic imaging. The vessel branching
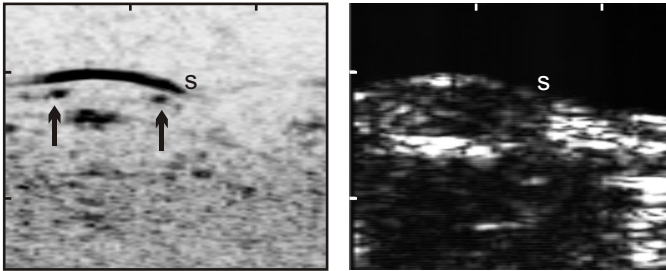
Figure 2: *In-vivo* optoacoustic image (left) and ultrasound image (right) of a human index finger (palm towards transducer). The images cover a 2.6 x 2.0 cm area. On the optoacoustic image (left) the skin is visible as an arc shaped black line (s). 1 mm below the skin the Vv. digitales palmares are visible as two black dots on either side of the finger (arrows). They are accompanied by the corresponding Aa. digitales palmares propriae, which appear much fainter (tiny dots besides veins) because of the reduced absorption of oxyhemoglobin at 760 nm wavelength. 3 mm below the skin, a blood perfused region possibly the periosteum is visible. The four vessels and the periosteum are hard to see on the corresponding ultrasound image (right). The ultrasound image is predominated by the echo signal from the skin (s) and the large echo signal from the bone 5 mm below it. The skin surface position matches well on both images, it is however obvious that the two methods extract complementary information. In the lower part of the optoacoustic image the noise floor becomes visible because of the applied depth gain correction. The skin and blood vessels appear possibly enlarged by saturation effects of strong optoacoustic signals. The contrast of the ultrasound images was increased by gamma adjustment. This was not necessary for the optoacoustic images. The complete optoacoustic image was acquired in real-time with three 15 mJ laser pulses (3x continuous averaging).
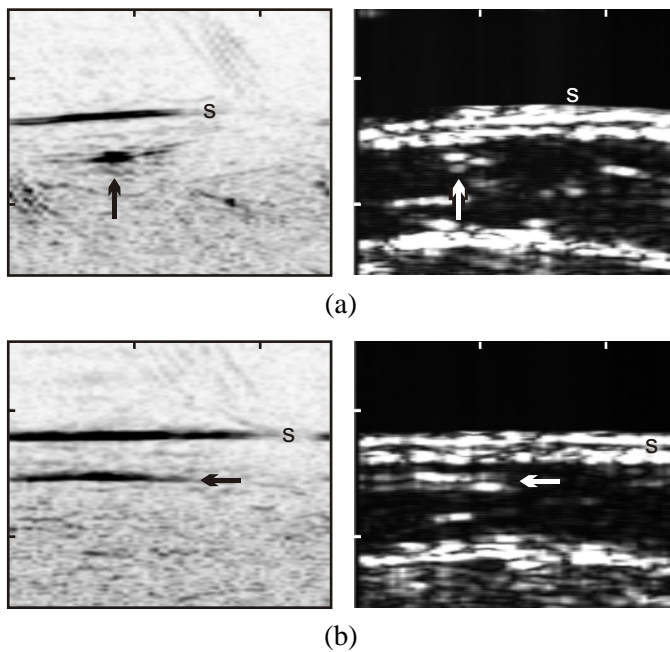
(a)

(b)

Figure 3: *In-vivo* optoacoustic images (left) and corresponding ultrasound images (right) of a vein at the interior part of the medial lower leg. The images cover a 2.6 x 2.0 cm area. (a) Cross section image from the interior part of the leg. In the optoacoustic image (left) the skin is visible as a black line (s). 4 mm below the skin a blood vessel (V. saphena magna) reveals itself as a pronounced black spot (arrow). The boundaries of the blood vessel are also visible in white on the ultrasound image (right) at the same location. Just right of the large vessel a smaller one is visible in the optoacoustic image. On the right half of the image approximately 8 mm below the skin another small blood vessel is visible in both images. (b) coronal configuration images acquired at the same position but with 90° turned transducer. The black upper line in the optoacoustic image (left) originates from the skin (s). The black line 4 mm below the skin (arrow) corresponds to the longitudinal section of the vein, which is also visible as two white lines in the ultrasound image (right). The contrast of the ultrasound images was increased by gamma adjustment. This was not necessary for the optoacoustic images. The optoacoustic images were acquired with a single 15 mJ laser pulse. No averaging was applied.

was easily traceable with the online system.

5   Discussion

While comparing optoacoustic imaging with classical ultrasound, some fundamental differences become obvious: (1) The contrast generation mechanism is different. Ultrasound contrast is based on acoustic properties, whereas optoacoustic contrast is based on optical properties. Optoacoustics therefore provides higher contrast and complementary information to classical ultrasound. (2) The two techniques have different regions of application. While ultrasound excels at depths up to 20 cm, optoacoustics focuses on the first centimeters limited by the light penetration. (3) The acquisition time is different. A classical b-mode ultrasound image consists of about 100 single a-scans, each with focused transmission and reception. In optoacoustics a complete image can be acquired with a single exposure. The image acquisition time is therefore about 100 times faster than classical ultrasound. It is easy to rapidly acquire an optoacoustic frame in between two ultrasound frames.

One challenge associated with optoacoustic imaging is the strong light absorption in the skin. This absorption reduces the light penetrating into the tissue especially for dark or hairy skin and therefore reduces the produced acoustic signal amplitudes. The acoustic transient generated on the surface not only propagates to the transducer but also into the tissue. There it produces echo signals, which are overlaid on the optoacoustic signals and become predominant at a certain depth. One possibility to avoid these echo signals is a forward mode configuration with the illumination on the opposite side of the detection. However this technique is restricted to boneless body parts, such as female breast, that are accessible from two sides.

An alexandrite laser was chosen because of the high output energy, short pulse duration and appropriate wavelength. But it has a nice property we haven't explored yet — tunability. Alexandrite lasers are tunable from 700 – 800 nm wavelength because of their vibronic transitions. This wavelength region lies optimally in the so called diagnostic window (650 nm – 900 nm), which is the optical range allowing large imaging depths in biological tissue. Looking at the hemoglobin spectra, the alexandrite
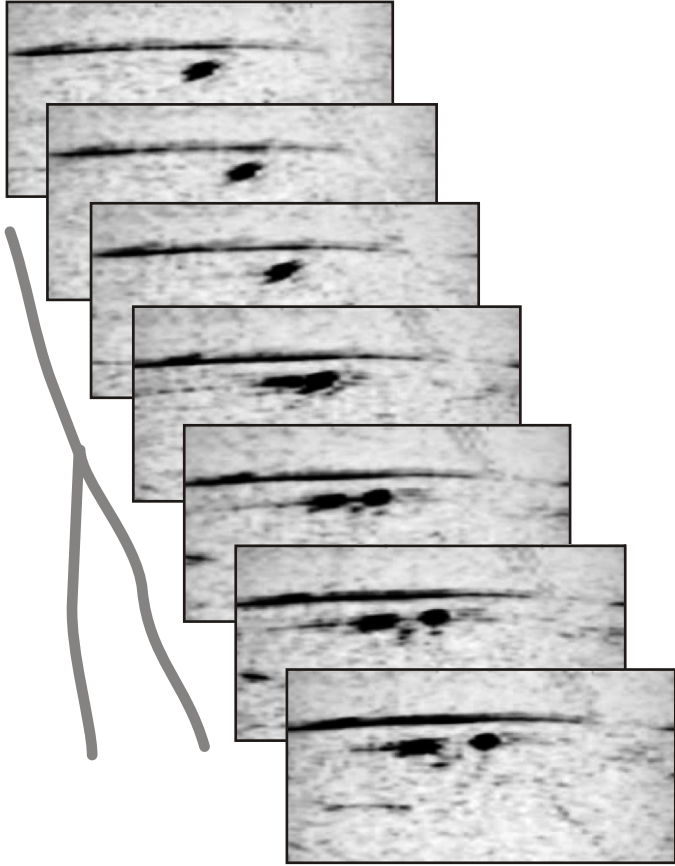
Figure 4: *In-vivo* optoacoustic images of a branching cutaneous vein in a human forearm. The image sequence was acquired by moving the transducer 1 cm along the forearm at a position 8 cm away from the wrist. The skin is visible as a black line in the upper part of all the images. The blood vessel is visible 2 mm below the skin as one spot branching into two spots on successive images. The optoacoustic images at 7.5 Hz repetition rate on the computer screen were recorded in a 4-second movie sequence. From this sequence 7 frames were extracted and stacked successively for this figure. The images cover a region of 2.6 x 1.3 cm. The laser pulse energy was 10 mJ. Two times temporal averaging was applied.

tuning region covers the isobestic point 800 nm where oxy- and deoxy-hemoglobin show identical absorption. At 760 nm deoxyhemoglobin absorption is stronger. With two optoacoustic images at these two wavelengths, a detailed blood oxygenation level image can be estimated.

We used a classical ultrasound system with minor modifications for our optoacoustic imaging setup. This large technical synergy and the large complementary image content of optoacoustics and ultrasonography strongly suggest a combined clinical device. Classical ultrasound images with overlaid optoacoustic information can potentially create a powerful new diagnostic device.

6   Conclusion

We presented an optoacoustic real-time imaging system based on an conventional ultrasound device and an alexandrite laser. *In-vivo* optoacoustic images from human finger, leg and arm showing the high contrast and detail are compared with ultrasound images. The results strongly suggest a combination of the two complementary techniques in a single device.

Acknowledgment

References

[1] C. G. A. Hoelen, F. F. M. de Mul, R. Pongers, and A. Dekker, "Three-dimensional photoacoustic imaging of blood vessels in tissue," *Optics Letters*, vol. 23, no. 8, pp. 648–50, 1998.

[2] A. A. Karabutov, E. V. Savateeva, N. B. Podymova, and A. A. Oraevsky, "Backward mode detection of laser-induced wide-band ultrasonic transients with optoacoustic transducer," *Journal of Applied Physics*, vol. 87, no. 4, pp. 2003–14, 2000.

[3] K. P. Kostli, D. Frauchiger, J. J. Niederhauser, G. Paltauf, H. P. Weber, and M. Frenz, "Optoacoustic imaging using a three-dimensional reconstruction algorithm," *IEEE Journal of Selected Topics in Quantum Electronics*, vol. 7, no. 6, pp. 918–23, 2001.

[4] K. P. Kostli and P. C. Beard, "Two-dimensional photoacoustic imaging by use of fourier-transform image reconstruction and a detector with an anisotropic response," *Applied Optics*, vol. 42, no. 10, pp. 1899–908, 2003.

[5] R. A. Kruger, Pingyu-Liu, Yuncai-Fang, and C. R. Appledorn, "Photoacoustic ultrasound (paus)-reconstruction tomography," *Medical Physics*, vol. 22, no. 10, pp. 1605–9, 1995.

[6] J. J. Niederhauser, D. Frauchiger, H. P. Weber, and M. Frenz, "Real-time optoacoustic imaging using a schlieren transducer," *Applied Physics Letters*, vol. 81, no. 4, pp. 571–3, 2002.

[7] J. A. Viator, B. Choi, M. Ambrose, J. Spanier, and J. S. Nelson, "In vivo port-wine stain depth determination with a photoacoustic probe," *Applied Optics*, vol. 42, no. 16, pp. 3215–24, 2003.

[8] G. Paltauf, H. Schmidt-Kloiber, K. P. Kostli, and M. Frenz, "Optical method for two-dimensional ultrasonic detection," *Applied Physics Letters*, vol. 75, no. 8, pp. 1048–50.

[9] R. G. M. Kolkman, E. Hondebrink, W. Steenbergen, and F. F. M. de Mul, "In vivo photoacoustic imaging of blood vessels using an extreme-narrow aperture sensor," *IEEE Journal of Selected Topics in Quantum Electronics*, vol. 9, no. 2, pp. 343–6, 2003.

[10] J. J. Niederhauser, M. Jaeger, and M. Frenz, "Comparision of laser-induced and classical ultrasound," *Proceedings of the SPIE The International Society for Optical Engineering*, vol. 4960, pp. 118–23, 2003.

[11] A. A. Oraevsky, A. A. Karabutov, S. V. Solomatin, E. V. Savateeva, V. G. Andreev, Z. Gatalica, H. Singh, and R. D. Fleming, "Laser optoacoustic imaging of breast cancer in vivo," *Proceedings of the*

SPIE The International Society for Optical Engineering, vol. 4256, pp. 6–15, 2001.

[12] Xueding-Wang, Yongjiang-Pang, Geng-Ku, G. Stoica, and L. V. Wang, "Three-dimensional laser-induced photoacoustic tomography of mouse brain with the skin and skull intact," *Optics Letters*, vol. 28, no. 19, pp. 1739–41, 2003.

[13] M. Frenz, G. Paltauf, and H. Schmidt-Kloiber, "Laser-generated cavitation in absorbing liquid induced by acoustic diffraction," *Physical Review Letters*, vol. 76, no. 19, pp. 3546–9, 1996.

[14] M. W. Sigrist, "Laser generation of acoustic waves in liquids and gases," *Journal of Applied Physics*, vol. 60, no. 7, pp. R83–121, 1986.

Appendix A

Acknowledgments

During a three-year project like this thesis, many people contribute in one or the other way. I am grateful for all the contacts and the received support during this valuable time.

First of all, I would like to thank Martin Frenz for his quality support on publishing papers, for the interesting scientific discussions and for providing a friendly working atmosphere in the group. I would also like to thank P. Niederer for his interest in the project and for supervising my work.

At the IAP I met many people who became very dear to me. Kornel Köstli, my predecessor, has contributed excellent work with his FFT reconstruction algorithm. Daniel Frauchiger was always available for a laugh and for Schlieren System discussions in the swimming pool. Michael Jaeger was a good discussion partner for scientific and personal things. I wish him all the best for his PhD work. I am glad that Sylvia Ulrich and Beat Kissling volunteered for the image experiments. Res Wüthrich, the mechanical assistant, was a great help for constructing the most complex things from a simple sketch. Especially at the beginning of my PhD I had enlightening discussions with H.P. Weber. Thanks to the whole IAP family.

In interdisciplinary projects medical advice is important. Prof. Schaffner, Prof. Mahler, Prof. Hunziker and Dr. Caliezi from the Insel Hospital were open for discussion and answered my questions about medical imaging. Frank Moser also provided me with medical jargon.

Also external contacts are crucial for such a project. Dieter Schweizer and Marc Liard from Kontron Ultrasound R&D were kind to lend me a commercial ultrasound system for my optoacoustic experiments. I also thank Peter Weber and Robert Lemor and the other people from the Fraunhofer Institute for the warm welcome during my one week stay in St. Ingbert and for providing the DiPhAS with all the necessary documentation. I met Jakob Jütz in Engelberg where we had good discussions on acoustic lens systems and realization thereof. Prof. Keppner from FH Le Locle supported us with the technology of ITO and parylene coating. The research was funded by the Swiss National Science Foundation (SNF).

My precious wife Sonja deserves special thanks. She had to endure my key ideas that often popped up at 2 a.m. in the morning and my absorption in thoughts related to my work. Sonja was a great support and encouragement for me. Last but most important I thank the Lord Jesus Christ for guidance and support throughout all the phases of this project.

Appendix B

Bibliography

Bibliography

[1] Xueding-Wang, Yongjiang-Pang, Geng-Ku, G. Stoica, and L. V. Wang, "Three-dimensional laser-induced photoacoustic tomography of mouse brain with the skin and skull intact," *Optics Letters*, vol. 28, no. 19, pp. 1739–41, 2003.

[2] J. A. Viator, B. Choi, M. Ambrose, J. Spanier, and J. S. Nelson, "In vivo port-wine stain depth determination with a photoacoustic probe," *Applied Optics*, vol. 42, no. 16, pp. 3215–24, 2003.

[3] M. C. Pilatou, N. J. Voogd, F. F. M. de Mul, W. Steenbergen, and L. N. A. van Adrichem, "Analysis of three-dimensional photoacoustic imaging of a vascular tree in vitro," *Review of Scientific Instruments*, vol. 74, no. 10, pp. 4495–9, 2003.

[4] B. P. Payne, V. Venugopalan, B. B. Mikic, and N. S. Nishioka, "Optoacoustic tomography using time-resolved interferometric detection of surface displacement," *Journal of Biomedical Optics*, vol. 8, no. 2, pp. 273–80, 2003.

[5] U. Oberheide, C. Lee, R. Krebs, H. Welling, W. Ertmer, and H. Lubatschowski, "Therapy monitoring of laser cytophotocoagulation by laser induced ultrasound," *Laser Physics*, vol. 13, no. 5, pp. 730–4, 2003.

[6] U. Oberheide, I. Bruder, H. Welling, W. Ertmer, and H. Lubatschowski, "Optoacoustic imaging for optimization of laser cyclophotocoagulation," *Journal of Biomedical Optics*, vol. 8, no. 2, pp. 281–7, 2003.

[7] S. J. Norton and Tuan-Vo-Dinh, "Optoacoustic diffraction tomography: analysis of algorithms," *Journal of the Optical Society of America A Optics, Image Science and Vision*, vol. 20, no. 10, pp. 1859–66, 2003.

[8] J. J. Niederhauser, M. Jaeger, and M. Frenz, "Comparison of laser-induced and classical ultrasound," *Proceedings of the SPIE The International Society for Optical Engineering*, vol. 4960, pp. 118–23, 2003.

[9] Minghua-Xu, Yuan-Xu, and L. V. Wang, "Time-domain reconstruction algorithms and numerical simulations for thermoacoustic tomography in various geometries," *IEEE Transactions on Biomedical Engineering*, vol. 50, no. 9, pp. 1086–99, 2003.

[10] K. P. Kostli and P. C. Beard, "Two-dimensional photoacoustic imaging by use of fourier-transform image reconstruction and a detector with an anisotropic response," *Applied Optics*, vol. 42, no. 10, pp. 1899–908, 2003.

[11] R. G. M. Kolkman, E. Hondebrink, W. Steenbergen, and F. F. M. de Mul, "In vivo photoacoustic imaging of blood vessels using an extreme-narrow aperture sensor," *IEEE Journal of Selected Topics in Quantum Electronics*, vol. 9, no. 2, pp. 343–6, 2003.

[12] A. Kharine, S. Manohar, R. Seeton, R. G. M. Kolkman, R. A. Bolt, W. Steenbergen, and F. F. M. de Mul, "Poly(vinyl alcohol) gels for use as tissue phantoms in photoacoustic mammography," *Physics in Medicine and Biology*, vol. 48, no. 3, pp. 357–70, 2003.

[13] A. A. Karabutov, E. V. Savateeva, and A. A. Oraevsky, "Optoacoustic tomography: new modality of laser diagnostic systems," *Laser Physics*, vol. 13, no. 5, pp. 711–23, 2003.

[14] V. G. Andreev, A. A. Karabutov, and A. A. Oraevsky, "Detection of ultrawide-band ultrasound pulses in optoacoustic tomography," *IEEE Transactions on Ultrasonics, Ferroelectrics and Frequency Control*, vol. 50, no. 10, pp. 1383–90, 2003.

[15] M. Yamazaki, T. Shimada, S. Sato, T. Miya, H. Ohigashi, H. Ashida, and M. Obara, "Characteristics of a photoacoustic detector for biomedical measurements," *Review of Laser Engineering*, vol. 30, no. 10, pp. 598–601, 2002.

[16] Xueding-Wang, Yuan-Xu, Minghua-Xu, S. Yokoo, E. S. Fry, and L. V. Wang, "Photoacoustic tomography of biological tissues with high cross-section resolution: reconstruction and experiment," *Medical Physics*, vol. 29, no. 12, pp. 2799–805, 2002.

[17] G. Paltauf, J. A. Viator, S. A. Prahl, and S. L. Jacques, "Iterative reconstruction algorithm for optoacoustic imaging," *Journal of the Acoustical Society of America*, vol. 112, no. 4, pp. 1536–44, 2002.

[18] A. A. Oraevsky and A. N. Oraevsky, "On a plasmon resonance in ellipsoidal nanoparticles," *Quantum Electronics*, vol. 32, no. 1, pp. 79–82, 2002.

[19] J. J. Niederhauser, D. Frauchiger, H. P. Weber, and M. Frenz, "Real-time optoacoustic imaging using a schlieren transducer," *Applied Physics Letters*, vol. 81, no. 4, pp. 571–3, 2002.

[20] K. P. Kostli, D. Frauchiger, J. J. Niederhauser, G. Paltauf, H. P. Weber, and M. Frenz, "Optoacoustic imaging using a three-dimensional reconstruction algorithm," *IEEE Journal of Selected Topics in Quantum Electronics*, vol. 7, no. 6, pp. 918–23, 2001.

[21] K. P. Kostli, M. Frenz, H. P. Weber, G. Paltauf, and H. Schmidt-Kloiber, "Optoacoustic tomography: time-gated measurement of pressure distributions and image reconstruction," *Applied Optics*, vol. 40, no. 22, pp. 3800–9, 2001.

[22] K. P. Kostli, M. Frenz, H. Bebie, and H. P. Weber, "Temporal backward projection of optoacoustic pressure transients using fourier transform methods," *Physics in Medicine and Biology*, vol. 46, no. 7, pp. 1863–72, 2001.

[23] G. Paltauf and H. Schmidt-Kloiber, "Pulsed optoacoustic characterization of layered media," *Journal of Applied Physics*, vol. 88, no. 3, pp. 1624–31, 2000.

[24] A. A. Karabutov, E. V. Savateeva, N. B. Podymova, and A. A. Oraevsky, "Backward mode detection of laser-induced wide-band ultrasonic transients with optoacoustic transducer," *Journal of Applied Physics*, vol. 87, no. 4, pp. 2003–14, 2000.

[25] C. G. A. Hoelen and F. F. M. de Mul, "Image reconstruction for photoacoustic scanning of tissue structures," *Applied Optics*, vol. 39, no. 31, pp. 5872–83, 2000.

[26] J. D. Hamilton, T. Buma, M. Spisar, and M. O'Donnell, "High frequency optoacoustic arrays using etalon detection," *IEEE Transactions on Ultrasonics, Ferroelectrics and Frequency Control*, vol. 47, no. 1, pp. 160–9, 2000.

[27] G. Paltauf, H. Schmidt-Kloiber, K. P. Kostli, and M. Frenz, "Optical method for two-dimensional ultrasonic detection," *Applied Physics Letters*, vol. 75, no. 8, pp. 1048–50, 1999.

[28] R. O. Esenaliev, A. A. Karabutov, and A. A. Oraevsky, "Sensitivity of laser opto-acoustic imaging in detection of small deeply embedded tumors," *IEEE Journal of Selected Topics in Quantum Electronics*, vol. 5, no. 4, pp. 981–8, 1999.

[29] C. G. A. Hoelen, F. F. M. de Mul, R. Pongers, and A. Dekker, "Three-dimensional photoacoustic imaging of blood vessels in tissue," *Optics Letters*, vol. 23, no. 8, pp. 648–50, 1998.

[30] Yuncai-Fang, "Photoacoustic ultrasonography and its potential application in mammography," *Medical Physics*, vol. 24, no. 10, p. 1647, 1997.

[31] G. Paltauf and H. Schmidt Kloiber, "Measurement of laser-induced acoustic waves with a calibrated optical transducer," *Journal of Applied Physics*, vol. 82, no. 4, pp. 1525–31, 1997.

[32] A. A. Oraevsky, S. L. Jacques, and F. K. Tittel, "Measurement of tissue optical properties by time-resolved detection of laser-induced transient stress," *Applied Optics*, vol. 36, no. 1, pp. 402–15, 1997.

[33] Shun-Lee, T. Anderson, Hong-Zhang, T. J. Flotte, and A. G. Doukas, "Alteration of cell membrane by stress waves in vitro," *Ultrasound in Medicine and Biology*, vol. 22, no. 9, pp. 1285–93, 1996.

[34] A. A. Karabutov, N. B. Podymova, and V. S. Letokhov, "Time-resolved laser optoacoustic tomography of inhomogeneous media," *Applied Physics B Lasers and Optics*, no. 6, pp. 545–63, 1996.

[35] M. Frenz, G. Paltauf, and H. Schmidt Kloiber, "Laser-generated cavitation in absorbing liquid induced by acoustic diffraction," *Physical Review Letters*, vol. 76, no. 19, pp. 3546–9, 1996.

[36] R. A. Kruger, Pingyu-Liu, Yuncai-Fang, and C. R. Appledorn, "Photoacoustic ultrasound (paus)-reconstruction tomography," *Medical Physics*, vol. 22, no. 10, pp. 1605–9, 1995.

[37] R. A. Kruger, "Photoacoustic ultrasound," *Medical Physics*, vol. 21, no. 1, pp. 127–31, 1994.

[38] R. A. Kruger and Pingyu-Liu, "Photoacoustic ultrasound: pulse production and detection in 0.5pp. 1179–84, 1994.

[39] Q. X. Chen, R. J. Dewhurst, P. A. Payne, and B. Wood, "A new laser-ultrasound transducer for medical applications," *Ultrasonics*, vol. 32, no. 4, pp. 309–13, 1994.

[40] Q. X. Chen, A. Davies, R. J. Dewhurst, and P. A. Payne, "Photoacoustic probe for intra-arterial imaging and therapy," *Electronics Letters*, vol. 29, no. 18, pp. 1632–3, 1993.

[41] K. Hori, M. Suzuki, S. Tanda, and S. Saito, "In vivo analysis of tumor vascularization in the rat," *Jpn J Cancer Res*, vol. 81, no. 3, pp. 279–88, 1990.

[42] M. Scalerandi and B. C. Sansone, "Inhibition of vascularization in tumor growth," *Physical Review Letters*, vol. 89, no. 21, pp. 218101/1–4, 2002.

[43] B. M. Fenton and S. F. Paoni, "Oxygenation and vascular perfusion in spontaneous and transplanted tumor models," *Adv Exp Med Biol*, vol. 530, pp. 165–76, 2003.

[44] S. M. Evans and C. J. Koch, "Prognostic significance of tumor oxygenation in humans," *Cancer Lett*, vol. 195, no. 1, pp. 1–16, 2003.

[45] M. Hockel, B. Vorndran, K. Schlenger, E. Baussmann, and P. G. Knapstein, "Tumor oxygenation: a new predictive parameter in locally advanced cancer of the uterine cervix," *Gynecol Oncol*, vol. 51, no. 2, pp. 141–9, 1993.

[46] A. G. Bell, "On the production and reproduction of sound by light," *American Journal of Science*, vol. 20, pp. 395–324.

[47] V. Zeninari, B. Parvitte, D. Courtois, V. A. Kapitanov, and Y. N. Ponomarev, "Methane detection on the sub-ppm level with a near-infrared diode laser photoacoustic sensor," *Infrared Physics & Technology*, vol. 44, no. 4, pp. 253–61, 2003.

[48] K. Hatanaka, Y. Tsuboi, H. Fukumura, and H. Masuhara, "Nanosecond and femtosecond laser photochemistry and ablation dynamics of neat liquid benzenes," *Journal of Physical Chemistry B*, vol. 106, no. 12, pp. 3049–60, 2002.

[49] V. A. Kapitanov, Y. N. Ponomarev, K. Song, H. K. Cha, and J. Lee, "Resonance photoacoustic spectroscopy and gas analysis of gaseous flow at reduced pressure," *Applied Physics B Lasers and Optics*, no. 7, pp. 745–50, 2001.

[50] T. Hoshimiya, "Simulation of photothermally diffused images and a concept of holoscan in photoacoustic and optical-probe imaging," *Applied Optics*, vol. 33, no. 31, pp. 7251–7, 1994.

[51] M. W. Sigrist, "Laser generation of acoustic waves in liquids and gases," *Journal of Applied Physics*, vol. 60, no. 7, pp. R83–121, 1986.

[52] Q. Munir and H. P. Weber, "Fiberoptic sensor in a resonant optoacoustic cell," *Optics Communications*, vol. 52, no. 4, pp. 269–73, 1984.

[53] P. Perlmutter, S. Shtrikman, and M. Slatkine, "Optoacoustic detection of ethylene in the presence of interfering gases," *Applied Optics*, vol. 18, no. 13, pp. 2267–74, 1979.

[54] J. F. Power, "Inverse problem theory in the optical depth profilometry of thin films," *Review of Scientific Instruments*, vol. 73, no. 12, pp. 4057–141, 2002.

[55] T. Buma, M. Spisar, and M. O'Donnell, "High-frequency ultrasound array element using thermoelastic expansion in an elastomeric film," *Applied Physics Letters*, vol. 79, no. 4, pp. 548–50, 2001.

[56] J. Philip, "Photoacoustic microscopy: principles and practical realisation," *Journal of Pure and Applied Ultrasonics*, vol. 22, no. 1, pp. 1–9, 2000.

[57] A. C. Gracias, C. Kuranaga, J. R. Senna, and M. D. Silva, "Photoacoustic imaging of voids in direct wafer bonding," *Review of Scientific Instruments*, vol. 71, no. 4, pp. 1869–72, 2000.

[58] A. Minamide, S. Shida, and Y. Tokunaga, "Improved method for three-dimensional imaging in photoacoustic microscope," *Japanese Journal of Applied Physics, Part 1 Regular Papers, Short Notes & Review Papers*, vol. 38, no. 5.

[59] G. Paltauf, H. Schmidt-Kloiber, and M. Frenz, "Photoacoustic waves excited in liquids by fiber-transmitted laser pulses," *Journal of the Acoustical Society of America*, vol. 104, no. 2, pp. 890–7, 1998.

[60] U. Bernini, P. Mormile, A. Novellino, and P. Russo, "Photoacoustic imaging of layered microcircuits for non-destructive evaluation of sub-surface defects," *Journal of Materials Processing Technology*, vol. 54, no. 1.

[61] Y. Tokunaga and A. Minamide, "Development of scanning photoacoustic microscope," *Japanese Journal of Applied Physics, Supplement*, vol. 31, pp. 149–51, 1992.

[62] T. Sun and G. J. Diebold, "Generation of ultrasonic waves from a layered photoacoustic source," *Nature*, vol. 355, no. 6363, pp. 806–8, 1992.

[63] R. J. Dewhurst and Q. Shan, "Through-transmission ultrasonic imaging of sub-surface defects using non-contact laser techniques," *Optics and Lasers in Engineering*, vol. 16, no. 2.

[64] B. Koyuncu, "Photoacoustic imaging of subsurface features in metals," *Optics and Lasers in Engineering*, vol. 13, no. 1, pp. 17–26, 1990.

[65] D. A. Hutchins, D. Jansen, R. P. Young, C. Saleh, and S. L. Kramer, "Imaging defects with laser ultrasound," *Nondestructive Testing Communications*, vol. 5, no. 2.

[66] J. F. Zuccon and A. Mandelis, "High-frequency differential piezo-electric photoacoustic investigation of ion-implanted (100) silicon wafers via laser beam position modulation," *IEEE Transactions on Ultrasonics, Ferroelectrics and Frequency Control*, vol. 35, no. 1, pp. 5–13, 1988.

[67] D. A. Hutchins and J. H. Page, "Phase insensitive detection of laser-generated ultrasound," *Applied Physics Letters*, vol. 48, no. 5, pp. 323–5, 1986.

[68] J. Westel, G. C., "Ultrasonic-wave generation by harmonic heating in composite structures," *Applied Physics Letters*, vol. 41, no. 6, pp. 511–13, 1982.

[69] G. Veith, "High resolution photoacoustic microscopy on a surface acoustic wave device," *Applied Physics Letters*, vol. 41, no. 11, pp. 1045–6, 1982.

[70] G. Busse, "Optoacoustic and photothermal material inspection techniques," *Applied Optics*, vol. 21, no. 1, pp. 107–10, 1982.

[71] S. Perkowitz and G. Busse, "Far-infrared optoacoustic material probing and imaging," *Optics Letters*, vol. 5, no. 6, pp. 228–9, 1980.

[72] K. Wang, V. Burns, G. Wade, and S. Elliott, "Opto-acoustic trans-ducers for potentially sensitive ultrasonic imaging," *Optical Engi-neering*, vol. 16, no. 5, pp. 432–9, 1977.

[73] H. Kawai, "The piezoelectricity of poly(vinylidene fluoride)," *Japanese Journal of Applied Physics*, vol. 8, no. 7, pp. 975–6, 1969.

[74] L. F. Brown, "Design considerations for piezoelectric polymer ul-trasound transducers," *IEEE Transactions on Ultrasonics, Ferro-electrics and Frequency Control*, vol. 47, no. 6, pp. 1377–96, 2000.

[75] R. C. Weast, ed., *Handbook of Chemistry and Physics*. Cleveland, OH: CRC Press, 56 ed., 1976.

Appendix C

Curriculum vitae

Rebgasse 3   Phone ++41 61 921-5869
4410 Liestal   Fax   ++41 61 922-2030
Switzerland   E-mail j.n@switzerland.org

Joël J. Niederhauser

Objective   Research and development. Special interest in biomedical technology.

Education   2001–2004   Swiss Federal Institute of Technology Zürich, Switzerland
PhD Electrical Engineering
- Wrote thesis on "Real-time biomedical optoacoustic imaging."
- Developed combined laser and medical ultrasound system.
- Invented real-time 3D optoacoustic imaging device.
- Researched with Biomedical Photonics Division, University of Bern.
- Earned Didactic Teaching Certificate in 2003.

1996–2001   Swiss Federal Institute of Technology Zürich, Switzerland
MS Electrical Engineering GPA 5.76/6

2001   University of Pennsylvania   Philadelphia, PA, USA
- MS thesis "Prediction of Epileptic Seizures based on Depth-EEG."

1999   Georgia Institute of Technology   Atlanta, GA, USA
- Attended graduate study abroad program for one year. GPA 3.92/4.

Awards   1996   27th International Physics Olympiad   Oslo, Norway
- Received "Honourable Mention."

Experience   2000   Medivision, Comp. Nav. Surgery   Oberdorf, Switzerland
Engineering Intern
- Developed circuit board for gravity vector measurements.
- Redesigned tool interface for electromagnetic compatibility (EMC).

1998   Kontron, Ultrasound   Basel, Switzerland
Engineering Intern
- Evaluated functionality of a complex ultrasound system.
- Analyzed and debugged advanced printed circuit board (PCB).

1996   EM-Test   Reinach, Switzerland
Engineering Consultant
- Developed automated computer aided quality assurance system for EMC testing devices.

Personal   Born on the 4th of July, 1976.
Nationality: Swiss.
Languages: Fluent in English, German and French.
Skills include: PCB design, EPLD, C++, Java, Basic, Matlab.
Hobbies: Piano, windsurfing, camp counselor, mountain biking.

Publications J. J. Niederhauser et al.
"Laser-induced & classical ultrasound"   Proc. SPIE. 2003; 4960: 118-23.
"Real-time optoacoustic imaging ..."   Appl. Phys. Let. 2002; 81(4): 571-3.
"Detection of seizure precursors ..."   IEEE TBME. 2003; 50(4): 449-58.